The physics of the non-oxide perovskite superconductor $MgCNi_3$

2004 J. Phys.: Condens. Matter 16 R1237

(http://iopscience.iop.org/0953-8984/16/43/R01)

INSTITUTE OF PHYSICS PUBLISHING JOURNAL OF PHYSICS: CONDENSED MATTER

J. Phys.: Condens. Matter **16** (2004) R1237–R1276 PII: S0953-8984(04)81247-5

TOPICAL REVIEW

The physics of the non-oxide perovskite superconductor $MgCNi_3$

S Mollah

Department of Physics, Aligarh Muslim University, Aligarh 202002, India

E-mail: s.mollahm@lycos.com and smollah@rediffmail.com

Received 26 May 2004, in final form 29 July 2004
Published 15 October 2004
Online at stacks.iop.org/JPhysCM/16/R1237
doi:10.1088/0953-8984/16/43/R01

Abstract

The present review article discusses the physics of the non-oxide perovskite superconductor $MgCNi_3$ on the basis of theoretical and experimental results available on the material up to July 2004. It was discovered following on from the breakthrough of the finding of the MgB_2 superconductor at the beginning of 2001, which has subsequently been intensively studied; however, less attention has been paid to it due to its much lower superconducting transition temperature, T_c (∼8 K), as compared to that of MgB_2 ($T_c \sim 39$ K). But it has many interesting properties which need to be focused on to obtain an understanding of its complicated physics. Energy band calculations show that the density of states (DOS) at the Fermi level, $N(E_F)$, is dominated by Ni d states and there is a von Hove singularity in the DOS just below E_F (<50–120 meV). It is surprising that the conduction electrons in it are derived from partially filled Ni d states, which typically lead to ferromagnetism in metallic Ni and many Ni-based binary alloys. MgC_xNi_3 has a simple cubic perovskite structure with space group $Pm\bar{3}m$ and the lattice parameter a is ∼3.812 Å for $x \sim 0.97$ at ambient temperature and pressure. However, the $Ni_6(O_6)$ octahedron is locally distorted from those expected in the perfect cubic $Pm\bar{3}m$ form. The carbon atom of $MgCNi_3$ at the body centre is surrounded by six Ni atoms at the face centred positions and eight Mg atoms at the cube corners. The carriers in it are of electron type in the normal state, although theoretically they were predicted to be of hole type. T_c increases with increase of x in MgC_xNi_3, but generally decreases with Ni site doping with Co, Fe, Mn, Cu etc. Theoretically, the DOS peak should be greatly reduced by doping at the Mg or Ni site, which accounts for the reduced T_c. The T_c is found to increase with increase of the external pressure (P) at a rate of $dT_c/dP \sim 0.0155$ K kbar^{-1}, which is the same as that for the intermetallic RNi_2B_2C (R = rare earth) superconductors but about one order lower than that for MgB_2. The $T_c(P)$ result focuses our attention on the feature that $N(E_F)$ should increase with pressure due to the broadening of the energy level. Also, a controversial magnetoresistance

is reported. It has been observed that the electronic contribution is slightly higher than the lattice one in the normal state thermal conductivity. Specific heat and tunnelling spectroscopic studies indicate that this is an s-wave BCS-type weak/moderate coupling type-II superconductor, but this needs further confirmation as the penetration depth distinctly exhibits a non-s-wave BCS low temperature behaviour which theoretically suggests a d-wave superconductor.

Contents

1. Introduction

Since the discovery of the new intermetallic non-oxide perovskite superconductor $MgCNi_3$ by He *et al* [1], following on from that of MgB_2 [2], extensive experimental [3–48] and theoretical [47–69] studies have been carried out on it. It has a perovskite structure [1] like that of $CaTiO_3$ with equivalence of Ca to Mg, Ti to C and O to Ni. Its structure is also like that of the 30 K non-cuprate oxide cubic superconductor [1] $Ba_{1-x}K_xBiO_3$. The high proportion of Ni in this compound suggests that magnetic interactions may play a dominant role in explanations of its superconductivity. In fact, the density of states (DOS) in the vicinity of the Fermi level is dominated by the Ni d states [49–54], though it is not large enough to induce magnetic instability [51] but is associated with the superconducting properties [53]. Ni K-edge x-ray absorption measurements [16] reveal that the $Ni_6(O_6)$ octahedra are locally distorted from those expected for the perfect cubic $Pm\bar{3}m$ form and electronic states in the vicinity of the Fermi level are mostly derived from the Ni d states and are degenerate. Experimental

investigation and theoretical computation reveal that there is a von Hove singularity (vHs) of the DOS just below E_F (<50–120 meV) [15, 54]. These bands are very narrow as they cannot disperse about the many points of high symmetry in the simple cubic Brillouin zone [50]. The degeneracy in the structure can be lifted by small perturbations such as electron–phonon (e–ph) interactions and lowering of the symmetry from cubic through Peierls-type transitions. The ^{13}C NMR investigation on this material [3] suggests that the electronic states reach modestly mass enhanced Fermi-liquid-like states prior to the superconducting transition. Evident structural inhomogeneity was detected by Li *et al* [7], with the appearance of regular superconducting domains of average size ∼4 nm. The temperature dependence of the structural parameters revealed by neutron diffraction study shows that there are no unusual changes in these [5] near T_c. The covalent character of the Ni–C bond implies that although most of the amplitude of the electron wavefunction resides on the Ni d, there might be spatial distribution of charge and spin governed by the Ni–C hybridization and Coulomb and e–ph interactions [70]. Lattice distortion associated with charge density waves (CDW) and long range antiferromagnetic (AF) ordering consistent with spin density waves (SDW) are not revealed in $MgCNi_3$ [1, 5]. Single-phase perovskite structure in MgC_xNi_3 is found [12] only in a narrow range of carbon content ($0.88 < x < 1.0$). The doping of the Ni site with Cu and Co decreases T_c significantly [6, 10]. Rosner *et al* [54] have suggested that $MgCNi_3$ is near a ferromagnetic instability that can be reached by hole doping on the Mg site (if 12% Mg is replaced by Na or Li, i.e., 0.04 hole/Ni) and the effective carriers are Ni-derived holes of very high band mass although the Hall coefficient and thermoelectric power data show that the carriers in this superconductor are electrons [4, 7]. Shein *et al* [53] have shown theoretically the deterioration of the superconducting characteristics of $MgCNi_3$ that occurs upon hole doping in $MgC_{1-x}Ni_3$ compositions. No magnetic solution is found for $MgCNi_2Co$ and $MgCNiCo_2$ [56]. This indicates that the hole doping does not produce a magnetic instability which could be responsible for pair breaking [56]. The decline of the superconductivity upon electron doping ($MgCNi_{3-x}Cu_x$) is due to the filling of antibonding states and a sharp drop in DOS at the Fermi level, $N(E_F)$ [53]. Thus there are many interesting properties of this non-oxide perovskite superconductor. The present review discusses the synthesis of $MgCNi_3$ along with its electronic, magnetic, thermal, mechanical and optical properties in the light of experimental findings and theoretical computations.

2. Synthesis of $MgCNi_3$

2.1. Polycrystalline bulk

MgC_xNi_3 samples with $x = 0.9$–1.5 were prepared by He *et al* [1] using as raw materials Mg flakes, fine Ni powder and glassy spherical carbon powder. The starting materials were properly mixed and pressed into pellets. The pellets were placed into Ta foil, put in an alumina boat and fired in a quartz tube furnace in a mixed gas (95% Ar and 5% H_2) environment. The samples were heat treated at 600 °C for 1/2 h and this was followed by treatment for 1 h at 900 °C. Then these were cooled, ground, pressed and heated at 900 °C for one more hour. Owing to the volatility of Mg, 20% excess of its stoichiometric ratio was added to the initial mixture. The preparation procedures of other groups are almost the same as that of He *et al* [1], as shown in table 1. Although most of the groups used Mg flakes, Ni powder and glassy C powder as raw materials with the final heat treatment temperature as 900 °C and Ta foil for wrapping or positioning the sample, there is a lot of variation as regards the starting mixture of raw materials, the final heat treatment time and the annealing environment (table 1). For example, Li *et al* [4, 7] prepared a sample with nominal formula $Mg_{1.2}C_{1.4}Ni_3$ in a stainless steel reactor under

Table 1. Summary of different recipes for the synthesis of $Mg_xC_yNi_3$ superconductor. Mg flakes, Ni powder and glassy C powder are used as the starting raw materials. Only the final heat treatment time, temperature and environment are shown. Ta foil was used by different groups either to wrap the sample or to place the sample on.

x	y	Annealing time (h)	Annealing temperature (°C)	Annealing environment	References
1.0	0.9–1.5	2	900	95% Ar + 5% H_2	[1]
1.2	1.4	2	900	Ar	[4, 7]
1.0–1.3	0.7–1.55	2	900	95% Ar + 5% H_2	[8]
1.0	1.0	3	900	Vacuum	[13]
1.2	1.45	2	900	Vacuum	[15]
1	1.45	8	900	Ar	[19]
1.0	1.0	3	900	Vacuum	[23]
1.2	1.6	—	900	Ar	[24]
0.5–1.55	1.0	4–30	850–1000	Vacuum	[28, 47]
0.75–1.55	0.85–1.45	4–30	850–1000	Vacuum	[28, 47]

an Ar atmosphere in a glove box. A heat treatment like that of He *et al* [1] in a tube furnace under Ar resulted in dense samples of length 7 mm and width 2 mm. Lin *et al* [13] started with the appropriate stoichiometric ratio, but added 20% excess of Mg over its stoichiometric ratio and the final pellets were annealed at 900 °C for 3 h in an evacuated quartz tube. The nominal composition of $MgC_{1.45}Ni_3$ was sintered at 900 °C for 8 h in flowing argon [19]. Kim *et al* [15] mixed powder with the nominal composition $Mg_{1.2}C_{1.45}Ni_3$. This was heated at 900 °C for 2 h and quenched. Afterwards, they [15] put the sample in a high pressure cell and annealed it under a pressure of 3 GPa at 900 °C for 1/2 h to get a dense sample for photoemission spectroscopy (PES) and x-ray absorption spectroscopy (XAS) studies. Bulk alloy samples of $Mg_xC_yNi_3$ ($1.0 < x < 1.3, 0.7 < y < 1.55$) were prepared by Li *et al* [8] using the conventional method [1]. Despite the fact that most of the groups used the final annealing temperature of 900 °C (table 1), there are some reports of synthesis with a temperature of 850–1000 °C [28, 47]. Non-superconducting α-MgC_xNi_3 and superconducting β-MgC_xNi_3 phases are found in the MgC_xNi_3 system for $x < 1.0$ and $x > 1.0$ [28] respectively, depending on the annealing temperature. Non-superconducting α-MgC_xNi_3 with $x < 1.0$ was prepared at a temperature lower than 965 °C. However, superconducting β-MgC_xNi_3 exists for $x > 1.0$, prepared at a temperature of 900–985 °C, and for $x < 1.0$, prepared at a temperature higher than 965 °C. MgC_xNi_3 ($x = 0.5$–1.55) and $Mg_xC_yNi_3$ ($x = 0.75$–1.55, $y = 0.85$, 1.0 and 1.45) systems were synthesized in an evacuated quartz tube placed in a box furnace and heated to the designed temperature (850–1000 °C) for 4–30 h; this was followed by furnace cooling to room temperature [28, 47]. In addition to being obtained by the conventional method [1], $MgCNi_3$ was synthesized from the Mg, Ni and graphite powders by mechanical alloying (MA), in which the preliminary condition for the formation of $MgCNi_3$ was the advance formation of Mg_2Ni [25]. $Mg_xC_yNi_3$ was prepared in two steps [26]; no evidence of Mg loss due to volatilization or of unreacted C was found at the end of the preparation. A new and feasible way to prepare $MgCNi_3$ under ambient conditions by ball milling (BM) Mg, Ni powder and paraffin or graphite was presented by Ouyang *et al* [44]. It was found that paraffin was partially dissociated during ball milling, which resulted in free carbon and hydrogen being incorporated within the Mg–Ni alloy powder in increasing amounts with increasing milling time. Recently, formation of transition metal boride and carbide perovskites related to superconducting $MgCNi_3$ in the ternary systems AXM_3 (A = Mg, Ca, Sc, Y, Lu, Zr, Nb; X = B; M = Ni, Ru, Rh, Pd, Pt) was reported by Schaak *et al* [27].

Table 2. Summary of different recipes for the preparation of $Mg_xC_yNi_{3-z}M_z$ (M = doping element) superconductor from Mg flakes, Ni powder, glassy C powder and M metallic powder. The final heat treatment temperature was 900 °C for all cases except those of [10] and [33]. Ta foil was used by different groups either to wrap the sample or to place the sample on.

x	y	z	M	Time (h)[a]	Atmosphere[a]	Excess Mg (%)	Excess C (%)	Max. T_c (K)	References
1.2	1.5	0.03–0.75	Co	2	95% Ar + 5% H_2	20	50	6.6	[6]
1.0	1.0	0.03–0.09	Cu	2	95% Ar + 5% H_2	20	50	6.5	[6]
1.0	1.45	0–3.0	Co	5	Vacuum	20	—	7.5	[10][b]
1.0	1.0	0.05–0.30	Fe	2	92% Ar + 8% H_2	20	50	8.5	[18]
1.0	1.0	0.05–0.40	Co	2	92% Ar + 8% H_2	20	50	7.7	[18]
1.0	1.0	—	Ag	2	Vacuum	—	—	6.6	[21]
1.2	1.5	0–0.05	Mn	7	Ar	—	—	—	[33][b]

[a] Final heat treatment time and atmosphere.
[b] The final heat treatment temperature is 950 °C.

2.2. *Chemical doping in $MgCNi_3$ polycrystalline bulk*

Chemical doping and diffusion of metallic particles in $MgCNi_3$ have been reported by several groups [6, 10, 18, 21, 33, 34, 36–38, 41]. The recipes for the syntheses by some groups are summarized in table 2. Most of the groups doped at the Ni site. However, the effect of doping at the Mg site is also studied [38, 41]. The preparation technique is over all conventional types [1]. Excess Mg and C in initial mixtures are found to be favourable for obtaining single-phase samples (table 2). $Mg_xC_yNi_{3-z}M_z$ (z = 0.05–0.30 and M = Fe, Co) were prepared [18] following the procedure of He *et al* [1] using the starting materials Mg, Ni, Fe, Co and amorphous carbon. Mg and C were taken with respectively 20% and 50% excess to get the required stoichiometry in the final sample. The final heat treatment atmosphere was also a little different (tables 1 and 2) to that of He *et al* [1]. $Mg_xC_yNi_{3-z}M_z$ (M = Cu, z = 0.03–0.09; M = Co, z = 0.03–0.75) samples were synthesized by Hayward *et al* [6] using the initial stoichiometry of $Mg_{1.2}C_{1.5}Ni_{3-x}M_x$. Ren *et al* [10] prepared Co doped (z = 0–3.0) samples in vacuum at a higher temperature (950 °C). Mn doped samples with x = 1.2, y = 1.5 and z = 0–0.5 (table 2) were synthesized at a slightly higher temperature with a higher heat treatment time in Ar [33]. Complete and partial replacement of Mg by Zn was carried out and $ZnCNi_3$ and $(Mg_{0.85}Zn_{0.15})CNi_3$ were prepared from the nominal compositions $Zn_{1.2}C_{1.3}Ni_3$ and $(MgZn)_{1.2}C_{1.3}Ni_3$, respectively, under a high purity Ar atmosphere [38, 41]. The pellets were reacted for 1 h at 900 °C, rapidly quenched to room temperature, then treated again for 2 h at 1000 °C. Excess Zn and C were used to compensate for the Zn evaporation during the reaction and to ensure full C incorporation, respectively. Ag diffused $MgCNi_3$ was synthesized by Liu *et al* [21] using stoichiometric $MgCNi_3$ pellets and a highly pure thin piece of Ag. These were wrapped in a Ta foil, sealed in a quartz tube, sintered at 900 °C for 2 h and cooled down to room temperature.

2.3. *Thin film*

So far, there has been only one report on the preparation of $MgCNi_3$ as a thin film [20]. The metastable intermetallic CNi_3 precursor films were deposited onto sapphire substrates by electron beam evaporation of CNi_3 targets. High purity graphite and nickel were used as the buttons, with initial composition $CNi_{3.25}$, to avoid the loss of Ni during the melting process. The films were grown with a typical growth rate $\sim$0.1 nm s^{-1} in a vacuum of 2 μTorr at room temperature and were handled in air. The adherent and pristine CNi_3 films were subsequently

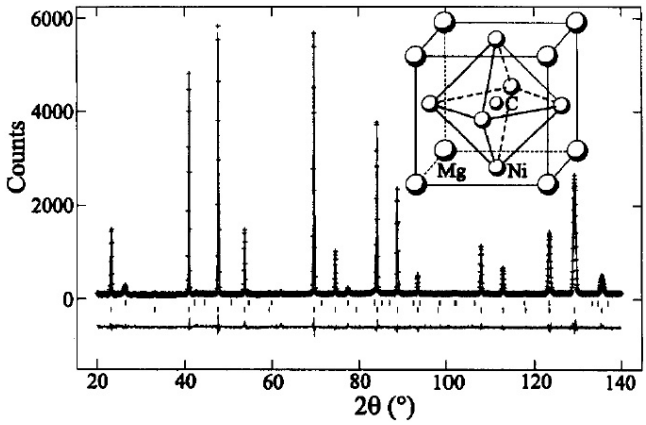

Figure 1. The powder neutron diffraction pattern at ambient temperature for $MgC_{1.25}Ni_3$; the inset shows the crystal structure of $MgCNi_3$ [1].

exposed to Mg vapour at 700 °C by sealing in a quartz tube in vacuum with 0.1 g of Mg metal. The entire quartz tube was rapidly quenched after heating for 20 min leading to the $MgCNi_3$ thin film formation.

It should be noted that although polycrystalline $MgCNi_3$ has been extensively studied in the form of bulk or thin film, it has not yet been investigated in the form of single crystal or wires/tapes. Thus there is immense scope for research focusing on the changes of properties (if any) in the above-mentioned form compared to those of the polycrystalline bulk and thin films.

3. The spectroscopic characterization and structure of $MgCNi_3$

This intermetallic $MgCNi_3$ superconductor is found to possess the classical cubic perovskite structure with the space group $Pm\bar{3}m$ and the lattice constant $a \sim 3.81221$ Å at 295 K [1, 5, 14, 21, 29]. Its neutron diffraction pattern and the atomic positions of the unit cell are shown in figure 1. From neutron diffraction study, it is found [1, 5] that the formula for the superconducting phase is $MgC_{0.96}Ni_3$ for the nominal composition $MgC_{1.25}Ni_3$. This is due to the small amount of unreacted graphite found in the sample [1, 5]. The C site occupancy is also found to be 0.960(8), by Ren *et al* [10]. The positions of the atoms are: Mg 1a (0, 0, 0); C 1b (0.5, 0.5, 0.5); Ni 3c (0, 0.5, 0.5), respectively with temperature factors 0.90(3), 0.54(4) and 0.75(1) $Å^2$ [1, 5]. Figure 2 shows the x-ray diffraction (XRD) spectrum of $MgCNi_3$ with unreacted Ni peaks. $Mg_xC_yNi_3$ ($1.0 < x < 1.3$, $1.0 < y < 1.55$) samples reveal evident structural inhomogeneity [8]. Regular domains, with an average size as small as ∼4 nm, appear commonly in the superconducting phase [8]. This structural phenomenon is qualitatively explained in terms of the perovskite cubic structure of $MgCNi_3$, modulated locally by the variable stoichiometry on the C sites. The presence of the local C deficiency can be a dominant factor affecting the crystal structure and superconductivity. Single-phase perovskite structure is found only in a narrow range of carbon content, $0.88 < x < 1.0$, in MgC_xNi_3 [12]. The introduction of carbon vacancies has significant effects on the positions of the Ni atoms. No evidence for long range magnetic ordering is observed by means of neutron diffraction for carbon stoichiometries within the perovskite phase stability range [12]. No homogeneous region with changeable content of Mg exists in $Mg_xC_yNi_3$ ($x = 0.75$–1.55 and $y = 0.85$–1.45) systems [28]. The electronic structure of $MgC_{1-x}Ni_3$ obtained by x-ray photoemission spectroscopy (XPS) and x-ray absorption spectroscopy (XAS) shows that the overall band structure is in reasonable agreement with band structure calculations, including

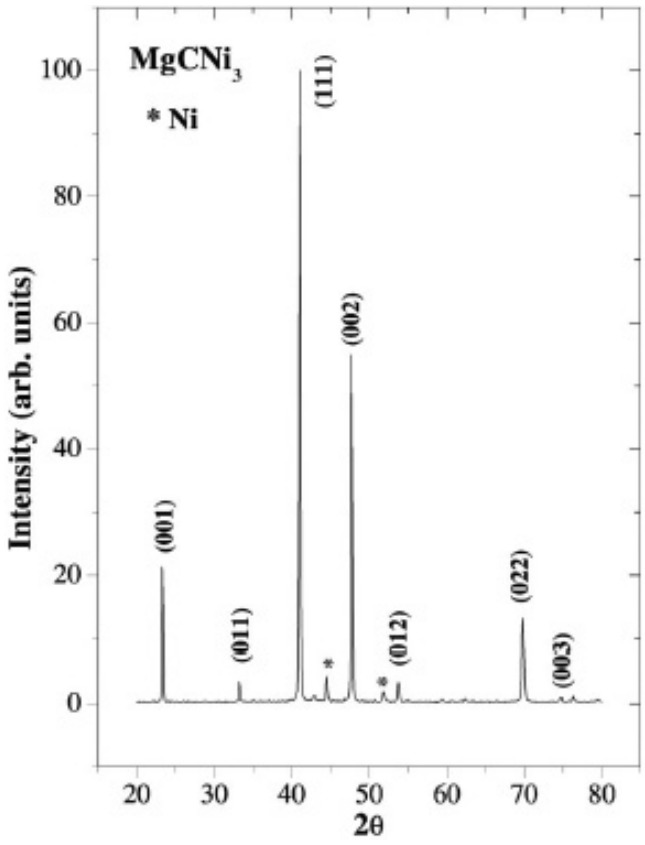

Figure 2. The x-ray diffraction pattern of pristine $MgCNi_3$. The lines marked with an asterisk correspond to unreacted Ni [18].

the existence of a von Hove singularity (vHs) near E_F [15]. However, the sharp vHs peak predicted theoretically near E_F [54] is substantially suppressed. As for the Ni core level and absorption spectrum, there exist satellites of Ni 2p which have a slightly larger energy separation and reduced intensity compared to the case for Ni metal [15]. These facts indicate that correlation effects among Ni d electrons may be important for understanding various physical properties. The onset of local distortions can be closely related to the removal of the degeneracy in the electronic states dominated by the Ni d bands [16]. The validity of the band structure calculations is confirmed by x-ray emission (C Kα, Ni $L_{2,3}$ and Co $L_{2,3}$) and x-ray photoelectron spectra [56].

In the $MgC_{1.45}Ni_{3-x}Co_x$ system [10], the lattice parameter decreases slightly with increasing x (figure 3). Thus, Shein *et al* [56] have used the same lattice parameter for all Co doped $MgCNi_3$ compounds because the changes in the lattice parameter from $MgC_{1.45}Ni_3$ to $MgC_{1.45}Co_3$ are found to be negligible [10]. Kumary *et al* [18] also find no significant changes of lattice parameter upon partial replacement of Ni with Fe or Co. It should be noted that *in situ* high pressure energy dispersive x-ray diffraction has also revealed that the structure of $MgCNi_3$ is stable under a pressure of $\sim$22 GPa [30]. Therefore, the chemical and the external pressure have the same effect on the lattice parameter [10, 15, 18, 30]. It decreases by only about 1% with Ag diffusion [21]. The XRD spectrum of Ag–$MgCNi_3$ also exhibits a series of Ag crystal peaks [21] corresponding to the known cubic structure with the lattice parameter 4.1065 Å. The XRD results show that a small amount of Ag is substituted at Ni sites, and much of the Ag is in vacancy sites of the Ag diffused $MgCNi_3$ [21]. Actually, the

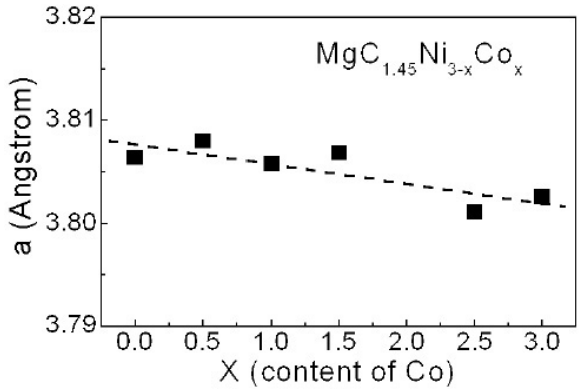

Figure 3. Lattice parameter versus x for the nominal composition $MgC_{1.45}Ni_{3-x}Co_x$ [10].

Ag is mostly located at the grain boundaries. The volume fraction of Ag on the surface of the samples is estimated at about 7.7% from XRD studies [21]. Raman spectroscopy reveals that Ag–$MgCNi_3$ has a special Raman peak at around 842.1 cm^{-1} compared to that of C [21]. The surface properties of Ag–$MgCNi_3$ have been studied using Raman scattering spectra and x-ray photoemission spectra (XPS) [21]. The coexistence of metal magnesium and magnesium oxide in the surface areas of Ag–$MgCNi_3$ is consistent with the results obtained from transmission electron microscopic (TEM) analysis.

Huang *et al* [5] report the structural parameters of superconducting MgC_xNi_3 ($x = 0.96$, $T_c = 7.3$ K) as a function of temperature, from 2–295 K, as determined by neutron powder diffraction profile refinement. It is established that the compound has the perovskite structure over the whole temperature range and no structural or long range magnetic ordering transitions are observed [5]. There are no unusual changes of the structural parameters near T_c [5]. This is also confirmed by the Ni K-edge x-ray absorption fine structure (EXAFS) over the temperature range of 3–300 K, which exhibits no anomaly near $T_c \sim 7$ K [16]. However, the symmetry of Ni_6 octahedra below the temperature $T^* \sim 70$ K is lower than cubic $Pm\bar{3}m$ [16]. Both the uniform spin susceptibility and the spin fluctuations show a strong enhancement with decreasing temperature and saturate below ∼50 and 20 K, respectively, as observed from ^{13}C nuclear magnetic resonance (NMR) characterization [3]. The lattice parameter a and the Debye–Waller factors for the individual atoms decrease smoothly with decreasing temperature. The lattice parameter a_T at any temperature T can be fitted with [5]

$$a_T = a_0 + \alpha T + \beta T^2, \tag{1}$$

where $a_0 = 3.8066$ is the value of a at $T = 0$ K; α (=3.7985×10^{-6}) and β (=5.3493×10^{-8}) are the polynomial coefficients. The thermal expansion of the model parameter cannot be fitted, unlike that for MgB_2 superconductor, with a model where the behaviour is dominated by a single phonon energy [52], which is expected as the strongly bonded network of light atoms (B) present in MgB_2 is absent in $MgCNi_3$. Thus there is the trend of decreasing lattice parameter with decrease of the temperature and increase of the Co doping [5, 10] although the effect of Co doping is negligible.

4. Electrical properties

4.1. The critical temperature (T_c)

The critical temperature (T_c) of a superconductor is determined as the average of the onset and end point temperatures. The upper part of figure 4 shows the temperature variation

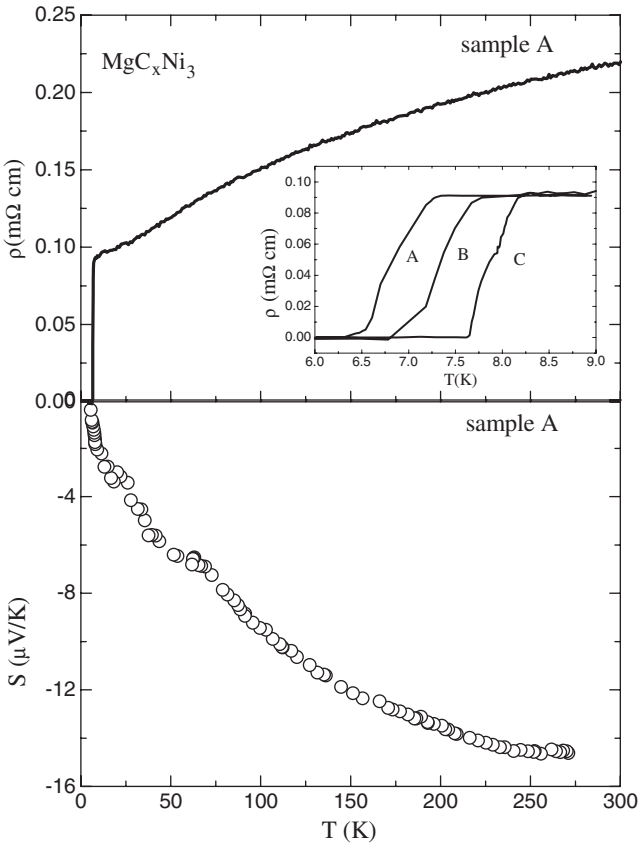

Figure 4. The temperature (T) variation of the resistivity (ρ) and the thermoelectric power (S) for sample A ($MgCNi_3$) at ambient pressure. The inset shows the resistivity (ρ) for the three MgC_xNi_3 samples with $x = 1.0$ (A), $x = 1.25$ (B) and $x = 1.5$ (C) near T_c [17].

of the resistivity for MgC_xNi_3 samples for $x = 1$ (A), 1.25 (B) and 1.5 (C). He *et al* [1] observe T_c from resistivity measurements for a sample with nominal composition $MgC_{1.5}Ni_3$ as 8.4 K with the onset temperature as 8.5 K and a 90%–10% transition width at 0.1 K. The T_c onset of the same sample is found from magnetization measurements as 7.4 K, whereas that from specific heat (C) studies is 6.1 K. Differences among the values of T_c derived from resistivity, magnetization and specific heat measurements are also found by several other groups [4, 7, 13, 17]. Different values of T_c being obtained by different techniques is also a well known fact for other intermetallic and oxide superconductors; they mainly depend on the sample homogeneity and transition width. Young *et al* [20] report on the T_c of $MgCNi_3$ thin films with thickness 7.5–60 nm (figure 5). Films thicker than ∼40 nm have $T_c \sim 8$ K, which is comparable to that of polycrystalline bulk samples. T_c decreases with decrease of the film thickness as shown in figure 5, becoming the minimum for the film with thickness 7.5 nm [20]. It should be mentioned that Artini *et al* [31] observe double superconductive transitions, with one ∼10 K higher than that (∼8 K) reported by others [1, 4, 7, 13, 17] and a second one at ∼6 K. In the following, the internal (chemical) and external pressure effects on the T_c of $MgCNi_3$ have been discussed.

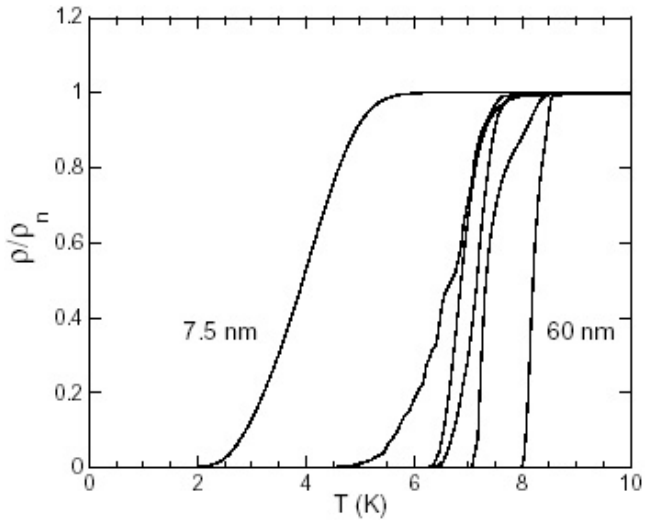

Figure 5. The temperature dependence of the resistivity for $MgCNi_3$ films with different thicknesses. The curves correspond from left to right to $MgCNi_3$ layer thicknesses of 7.5, 15, 20, 30, 45 and 60 nm [20].

4.1.1. The internal pressure (chemical doping) effect. The T_c of MgC_xNi_3 is sensitive to the carbon content as shown in table 3. The T_c varies from 6.4 to 8.4 K depending on the value of x (table 3). MgC_xNi_3 ($x = 1.0$–1.5) samples reveal an increase of T_c [17] with increase of x (figure 4). The highest T_c corresponds to $x \sim 1.45$–1.5 and decreases with further increase of x [1, 10, 11, 17, 19, 48]. The T_c is found to decrease systematically with decreasing carbon concentration [12] from the stoichiometric value. It is concluded from theoretical calculations that the absence of superconductivity for non-stoichiometric compositions $MgC_{1-x}Ni_3$ is due to the transition of the system to the magnetic state [53]. Excess of Mg and C in the initial material mixture is favourable for improving T_c and for obtaining single-phase samples [1, 10]. The T_c of $MgC_{1.45-x}B_xNi_3$ decreases with increase of x up to 0.10 and then it becomes non-superconducting for $x = 0.15$–0.20 [10]. The T_c of Ag–$MgCNi_3$ (~6.6 K) is lower than that of pure $MgCNi_3$ [21]. The complete replacement of Mg by Zn in $ZnCNi_3$ causes it to become paramagnetic without the onset of superconductivity down to ~2 K [38].

Doping at the Ni site with Co, Fe, Mn, Cu etc also causes a decrease of T_c (table 2)—except the initial increase with Fe doping [18]. Calculation of the expected electronic DOS suggests that electron (Cu) and hole (Co) doping should have different effects on T_c [6]. However, the T_c of $MgCNi_{3-z}Cu_z$ decreases systematically from 7 to 6 K for $z = 0.1$ [6]. It is also observed by other groups that both electron (Cu) and hole (Co, Fe and Mn) doping quench the superconductivity of $MgCNi_2T$ (T = Co, Fe, Mn and Cu) [36, 37]. Consequently, comparing with the hole (Co) doping, we see that there is not much difference between Cu and Co doping, which is opposite to what observed by Hayward *et al* [6]. As the metallic doping at the Ni site finally leads to non-superconducting phases, the maximum T_c of $Mg_xC_yNi_{3-z}M_z$ (M = metal) for lower metallic doping concentrations (z) is shown in table 2. The T_c of $MgC_{1.45}Ni_{3-z}Co_z$ decreases gradually with increasing z [10]. A small superconducting transition is observed for the sample with $z = 1.5$, which indicates that the superconducting volume fraction decreases upon substitution of Co for Ni. This is inconsistent with the finding of [6], where z above 0.03 completely suppresses the superconductivity. Kumary *et al* [18] also monitored the decrease of T_c with increase of the Co content. No magnetic solution was found for $MgCNi_2Co$ and $MgCNiCo_2$ [56]. This indicates that the hole doping does not produce the magnetic instability which could be responsible for pair breaking [56]. Again, no long range magnetic ordering is observed in the magnetic susceptibility of $MgCNi_{3-z}Co_z$ [6]. The Co doping of $MgCNi_3$ is

Table 3. Some important characteristic parameters of MgC_xNi_3.

Parameters[a]	Values of parameters								
x	1.0	1.0	1.5	1.6	1.0	1.0	1.4	1.0	1.0
T_c (K)	7.63	6.4	8.4	6.8	7.3	7	8	8	6.7
$H_{c2}(0)$ (T)	14.4	11.5	12.8	11.0	16	11.8	15	14	—
$H_c(0)$ (T)	0.19	0.29	—	0.18	0.6	—	—	—	—
$H_{c1}(0)$ (mT)	10	—	—	11.3	12.6	—	—	—	—
$\xi_{GL}(0)$ (Å)	46	56	50	54.7	45	—	47	50	—
$\lambda_{GL}(0)$ (Å)	2480	1800	—	2370	2300	—	—	—	—
$\kappa(0)$	54	—	66	43.3	51	—	—	—	—
γ_n (mJ K^{-2} (mol Ni)$^{-1}$)	10.03	11.2	10	10.5	—	11.3	—	—	9.8
θ_D (K)	284	287	—	292	—	351	206	—	256
n (10^{22} cm^{-3})	—	—	—	—	—	—	1.0	4.2	—
λ	—	0.83	0.77	0.84	—	0.66	1.4	—	0.79
$\Delta C/\gamma_n T_c$	2.1	1.97	1.9	2.09	—	1.7	—	—	—
$2\Delta/k_B T_c$	4.4	$\geqslant$4	—	3.75	—	$\sim$5	—	—	—
Δ (meV)	1.5	1.1	—	1.1	—	1.5	—	—	—
References	[9]	[13, 14]	[1, 11]	[48]	[23]	[47]	[4, 7]	[20]	[38]

[a] The symbols are explained in the text.

accompanied by a reduction of the DOS at the Fermi level, which seems to be responsible for the reduced superconductivity in the $MgCNi_{3-z}Co_z$ system [56]. An increase followed by a decrease of T_c is observed if Ni is replaced by Fe [18]. The maximum T_c is found by monitoring when the Fe concentration is 0.05. The authors of [18] argue that the spin fluctuation effect would be less for Fe substituted compounds as compared to that for Co substituted ones for low concentration of doping. The detected variation of T_c is explained in terms of the competition between an increase in T_c due to increase in the DOS and a decrease in spin fluctuation [18]. Conversely, Alzamora *et al* [34] find that the Fe doping in $MgC(Ni_{1-x}Fe_x)_3$ ($0 \leqslant x \leqslant 1.0$) quickly reduces T_c, completely destroying the superconducting state for $x \sim 0.04$. It is confirmed that Co and Fe dopants in $MgCNi_3$ behave as a source of d band holes [36, 37] and the suppression of superconductivity occurs faster for the Fe doped compared to the Co doped case, which is in contrast to the finding of Kumary *et al* [18]. So the above discussion suggests that doped Co and Fe do not act as magnetic impurities in $MgCNi_3$. On the contrary, the rapid loss of superconductivity for Co replacement of Ni is argued to be consistent with magnetic quenching of the superconductivity [6]. It is also suggested that Co is a very strong magnetic impurity rather than a source of hole doping [6], which is opposite to the observation of other groups [6, 18, 36, 37, 53, 56]. Again, the establishment of an ordered magnetic state is observed for Fe concentration ($z \geqslant 0.3$) far above the concentration for which the superconducting state has completely disappeared [34]. In addition, Das and Kremer [33] observe a rapid suppression of the superconductivity (~ -21 K/at.% Mn) in Mn substituted $MgCNi_3$. Doping with only 0.3 at.% of Mn completely destroys the superconductivity in $MgCNi_{3-z}Mn_z$ via pair breaking effects due to moment formation for Mn [33]. This is consistent with the observation of Ren *et al* [10] who find that the suppression effect is smaller for Co than for Mn, when replacing Ni. Thus the doping effect needs further investigation to settle the controversies.

4.1.2. The external pressure effect. High pressure (P) plays an important role as regards the T_c of the intermetallic superconductors [71–77]. The P can change the electronic structure, phonon frequencies and electron–phonon coupling, affecting the T_c. Isotropic pressure will not affect too much the electronic structure but anisotropic compression will cause large

Table 4. The superconducting transition temperature T_c (determined from the mid-point of the resistive transition for MgC_xNi_3) at ambient pressure, dT_c/dP and $d\ln T_c/dP$ for some metallic as well as some intermetallic superconductors.

Sample composition	T_c (K)	dT_c/dP (10^{-2} K kbar^{-1})	$d\ln T_c/dP$ (10^{-3} kbar^{-1})	References
MgB_2	38.6	−8.0	−2.07	[72]
MgB_2	37.5	−16.0	−4.26	[73]
$LuNi_2B_2C$	15.9	+1.88	+1.18	[75]
V	5.3	+1.0	+1.88	[81]
Ta	4.3	−0.26	−0.60	[82]
$MgCNi_3$	7.69	∼−1.0	∼−1.30	[18][a]
$MgCNi_3$	7.69	∼+0.75	∼+0.97	[18][b]
MgC_xNi_3 (A)	6.9	+1.55	+2.24	[17]
MgC_xNi_3 (B)	7.4	+1.34	+1.81	[17]
MgC_xNi_3 (C)	7.9	+1.52	+1.92	[17]

[a] Below the pressure of 17 kbar.
[b] Above the pressure of 17 kbar.

pressure induced changes due to the change of bonding strength in different crystallographic directions [71]. Yang *et al* [17] have measured the hydrostatic pressure dependent ac magnetic susceptibility (χ_{ac}) of MgC_xNi_3 using the piston–cylinder self-clamped technique [78]. The hydrostatic pressure environment around the sample is generated inside a Teflon cell with 3M Fluroinert FC-77 as the pressure-transmitting medium [17]. The pressure is determined by using a Sn manometer situated near the sample in the same Teflon cell [17]. On the other hand, a high pressure resistance measurement has been carried out [18] for pristine $MgCNi_3$ using a pressure locked, opposed Bridgman anvil apparatus [79] using the four-probe method. A superconducting Pb manometer is used for the pressure calibration [18].

An initial decrease in T_c of $MgCNi_3$ with $dT_c/dP \sim -1.0 \times 10^{-2}$ K kbar^{-1} up to a pressure of ∼17 kbar (table 4) followed by an increase is observed on application of external pressure, from resistivity measurements [18]. The decrease in T_c for small applied pressures is explained in terms of the decrease in the DOS at the Fermi level. The subsequent increase in T_c with pressure is argued to be due to a lattice softening or a structural phase transition, consistent with the band structure calculations. It is conjectured that suppression of spin fluctuations by pressure may also be responsible for the observed increase in T_c at higher pressures [18]. However, Yang *et al* [17] observe an increase of T_c with pressure from ac susceptibility measurements on three MgC_xNi_3 (for $x = 1.0$, 1.25 and 1.5) samples, which is in contradiction to the low pressure result of Kumary *et al* [18]. The temperature variation of the ac magnetic susceptibility (χ_{ac}) for different MgC_xNi_3 samples under pressure (0–17 kbar) is shown in figure 6. The T_c (mid-point) for the sample with $x = 1.0$ (sample A) increases from 6.56 to 6.79 K with increase of the pressure from ambient to 14.80 kbar, as illustrated in figure 7, at the rate of $dT_c/dP \sim 0.015$ K kbar^{-1}. A similar trend of the pressure effect on T_c for other samples [17] is also observed (table 4). This rate is slightly higher than that (∼0.0075 K kbar^{-1}) observed by Kumary *et al* [18] at pressures above 17 kbar. To give a clear idea of the pressure effect on T_c for other intermetallic and metallic superconductors such as MgB_2, $LuNi_2B_2C$, Ta and V [71–77, 80–82], some of the results are listed in table 4. Yang *et al* [17] explain the increase of T_c with pressure as follows.

The change of T_c with the unit cell volume (V) can be given by [71, 75]

$$(V/T_c)(dT_c/dV) = d\ln T_c/d\ln V = -(B/T_c)(dT_c/dP), \tag{2}$$

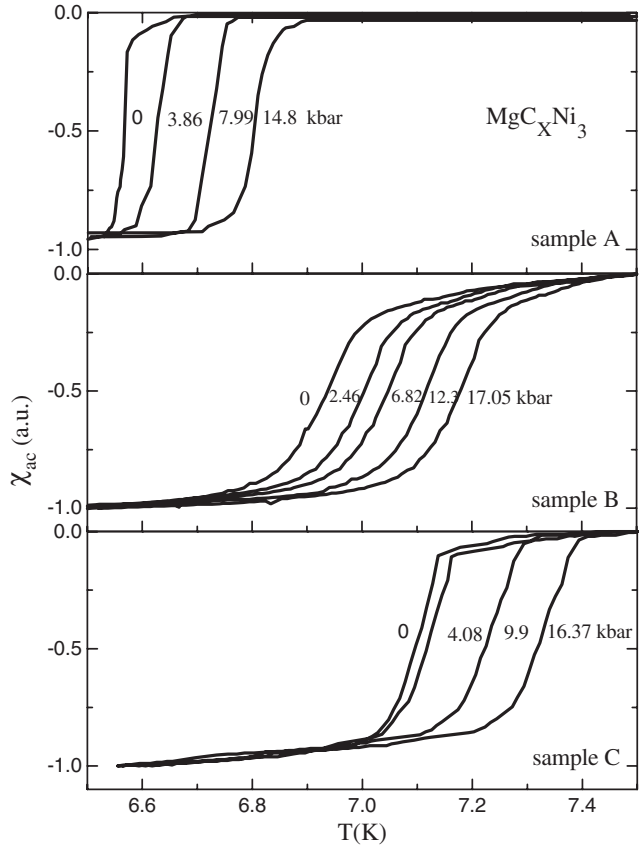

Figure 6. The variation of the ac magnetic susceptibility (χ_{ac}) of MgC_xNi_3 samples with $x = 1.0$ (A), 1.25 (B) and 1.5 (C) near T_c at various pressures (P) [17].

where B is the bulk modulus of the superconductor. Using the calculated value of B for MgC_xNi_3, 1510 kbar [18], and taking the dT_c/dP and T_c obtained from table 4, the $d\ln T_c/d\ln V$ values were found from equation (2); they vary from -3.18 to -2.58. These values are of the same order of magnitude for MgB_2 superconductor (+4.16), but with the opposite sign [71].

Since the DOS is sufficiently large in MgC_xNi_3 to produce strong electron–phonon coupling [51] and is supported by the thermoelectric power (S) data, the T_c can be expressed by the McMillan formula [80] as

$$T_c = (\theta_D/1.45)\ \exp\{-1.04(1+\lambda)/[\lambda - \mu^*(1+0.62\lambda)]\}, \tag{3}$$

where μ^* is the Coulomb pseudopotential and θ_D is the Debye temperature. λ is the electron–phonon coupling constant and is given by

$$\lambda = N(E_F)\langle I^2\rangle/M\langle\omega^2\rangle, \tag{4}$$

where $N(E_F)$ is the DOS at the Fermi level, $\langle I^2\rangle$ is the square averaged electronic matrix element for electron–phonon interaction, M is the ionic mass and $\langle\omega^2\rangle$ is the square averaged phonon frequency. It appears from equation (3) that the change of λ and θ_D caused by pressure will determine the sign of dT_c/dP. It is well established that the pressure induces lattice stiffening and generally reduces the T_c [75, 76]. However, the DOS effect can either

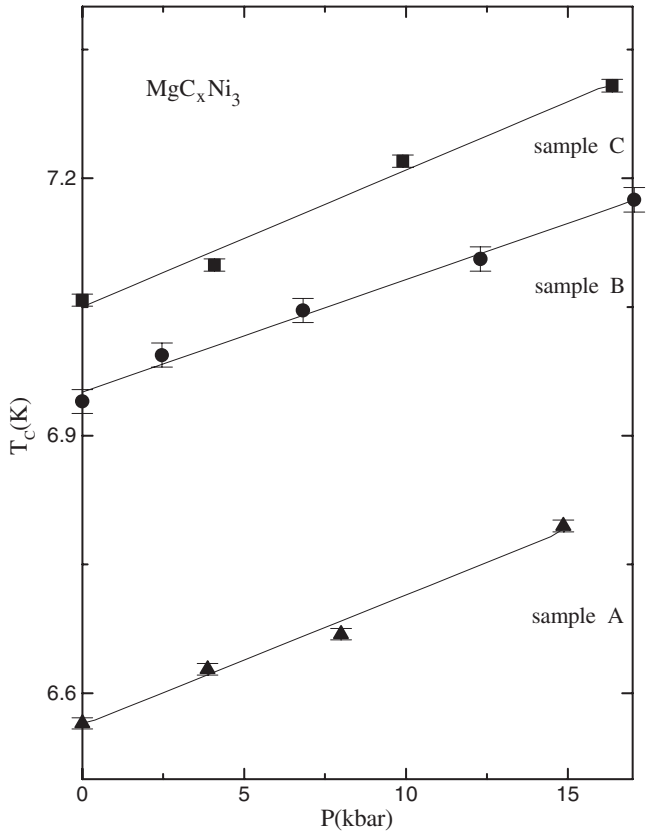

Figure 7. The pressure (P) dependence of the superconducting transition temperature (T_c) of MgC_xNi_3 samples with $x = 1.0$ (A), 1.25 (B) and 1.5 (C) [17].

enhance or reduce the T_c by, respectively, increasing or decreasing $N(E_F)$ on application of pressure [75, 76]. The dependence of T_c on θ_D is complicated as it appears both in the linear and in the exponent (being connected with $\langle\omega^2\rangle$ in equation (4)) terms of equation (3). Again, the change of exponent λ in equation (3) will be more effective than that of the linear term θ_D in determining T_c. Therefore, the positive dT_c/dP for MgC_xNi_3 possibly originates from the increase of $N(E_F)$ and consequently the enhancement of the electron–phonon coupling constant λ (equations (4)) if μ^* and $\langle I^2\rangle$ are less pressure dependent [17]. In addition, the P causes not only a shifting of the E_F but also a broadening of the energy bands. This broadening of the energy bands may also increase the $N(E_F)$. The computation of some important parameters such as $d\ln N(E_F)/dP$ and $d\ln\omega/dP$ of MgC_xNi_3 may be useful for quantitative analysis of the pressure dependent T_c data.

Yang *et al* [17] have also argued that the reduction of spin fluctuation with P may also be one of the reasons for the positive pressure effect on the T_c of MgC_xNi_3. Generally, the deficiency of carbon compared with the optimum value decreases the T_c [1, 8]. Non-stoichiometry of carbon (if any) may also affect the energy bands of the sample and alter the position of E_F compared to that expected from theoretical energy band calculations [49–54] for stoichiometric $MgCNi_3$. As the dT_c/dP is not changed much with carbon content, this suggests that the carbon deficiency does not significantly affect the pressure effect on T_c of MgC_xNi_3 [17]. The controversial results of Yang *et al* [17] as compared with those of Kumary *et al* [18] may be due to the reduction of grain boundary effects caused by pressure. Yang *et al* [17] claim that once the pressure applied is high enough ($\sim$17 kbar) to overcome the

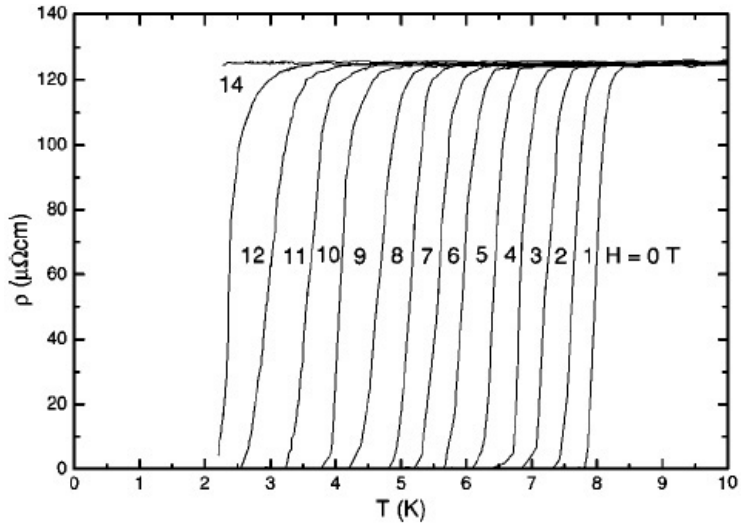

Figure 8. Resistivity versus temperature curves of $MgCNi_3$ at different fixed magnetic fields (H) [4].

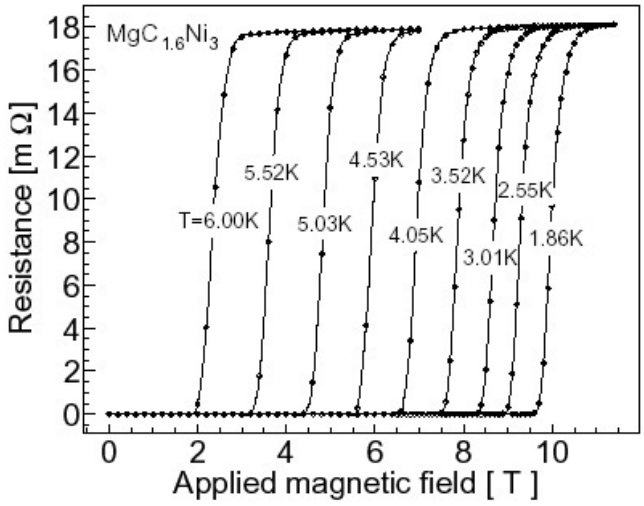

Figure 9. The field dependence of the resistivity of $MgC_{1.6}Ni_3$ measured at several fixed temperatures [48].

grain boundary effect, the bulk superconductivity dominates and the positive dT_c/dP is found the same as the observation of Kumary *et al* [18] using resistivity measurements. It should be mentioned that the effect of irradiation pressure on T_c is just opposite to that of hydraulic pressure [17, 32]. It has been found that the T_c of $MgCNi_3$ decreases from 6.5 to 2.9 K upon disordering induced by irradiation from a nuclear reactor and is completely restored after annealing at a temperature of 600 °C [32].

5. Magnetic properties

5.1. Critical fields (H_{c1} and H_{c2})

The upper critical field $H_{c2}(0)$ of $MgCNi_3$ is determined both from the specific heat (C) and from the resistivity (ρ) data [1, 4, 7, 9, 11–14, 20, 23, 47, 48, 83]. The results derived from ρ are nearly identical to those determined from the anomaly in C. Figure 8 shows the temperature

Table 5. Comparison between $MgCNi_3$, $Nb_{0.5}Ti_{0.5}$ and Nb. The parameters of $MgCNi_3$ are similar to those of $Nb_{0.5}Ti_{0.5}$ and Nb [13].

	$MgCNi_3$	$Nb_{0.5}Ti_{0.5}$	Nb
T_c (K)	6.4	9.3	9.2
$\Delta C/\gamma_n T_c$	1.97	∼1.9	1.87
$\ln(\theta_D/T_c)$	3.79	3.23	3.40
$2\Delta/k_B T_c$	⩾4	3.9	3.80
H_{c2} (T)	11.5	14.2	∼0.2
θ_D (K)	287	236	275
γ_n (mJ mol^{-1} K^{-2})	33.6 (11.2/Ni)	10.7	7.79

variation of ρ in different magnetic fields (H) up to 14 T [4]. The magnetic field dependence of the resistivity of $MgC_{1.6}Ni_3$ measured at several temperatures is illustrated in figure 9 [48]. The T_c decreases with increase of the magnetic field and finally becomes non-superconducting (figures 8 and 9). A magnetic field of 8 T leads to about 50% suppression of T_c and a complete suppression takes place at 14 T [4, 14]. The width $\Delta H = H_{90} - H_{10}$, with H_{90} and H_{10} being respectively the field values where 90% and 10% of the normal state resistivity is observed, remains constant at ∼0.6 T down to low temperature (figure 9). This indicates that $MgCNi_3$ has a small anisotropy in H_{c2}, as the strongly anisotropic superconductor shows a gradual broadening of the superconducting transition with decrease of the temperature [48]. The slopes $(dH_{c2}/dT)_{T_c}$ derived from the linear fits of both the C and the ρ data for $0.8 \leqslant (T/T_c) < 1$ are very close to each other [14]. The values of $(dH_{c2}/dT)_{T_c}$ are found as 2.96 ± 0.08 and 2.88 ± 0.03 T K^{-1} respectively from C and ρ measurements [13, 14]. Neglecting the spin–orbit interaction and the spin paramagnetic term in $MgCNi_3$, the relation

$$H_{c2}(0) \approx 0.69 T_c (dH_{c2}/dT)_{T_c} \tag{5}$$

leads to $H_{c2}(0) \sim 13.2 \pm 0.7$ T [14]. Similarly, $H_{c2}(0) = 14.8$ T is estimated from equation (5) by Mao *et al* [9]. As the spin–orbit and the spin paramagnetic effect are not taken into account, the value of $H_{c2}(0)$ is significantly overestimated [13]. It is found that the physical properties of $MgCNi_3$ [13] are very similar to those of $Nb_{0.5}Ti_{0.5}$ (table 5). Thus Lin *et al* [13] conclude that the two compounds may have similar relations between $H_{c2}(0)$ and $(dH_{c2}/dT)_{T_c}$. Again, $H_{c2}(0) \approx 0.59 T_c (dH_{c2}/dT)_{T_c}$ for $Ni_{0.5}Ti_{0.5}$ [13]. Following this relation, it is found that $H_{c2}(0) = 11.2 \pm 0.6$ T for $MgCNi_3$ [13]. The values of $H_{c2}(0)$ obtained by different groups vary from 11 to 16 T (table 3). The H_{c2} versus T curve of $MgCNi_3$ is shown in figure 10 [4]. Downward curvature in figure 10 indicates the conventional superconductivity in $MgCNi_3$. It is contended [16, 48] that $MgCNi_3$ has a Werthamer–Helfand–Hohenberg-like [84] temperature dependence of $H_{c2}(T)$ and follows the quadratic relationship

$$H_{c2}(0) = 0.0237(1 + \lambda)^{2.2} T_c^2/(10^5 \times v_F^2), \tag{6}$$

with v_F as the bare Fermi velocity, which points to an effective predominant single-band behaviour near the quasi-clean limit [85]. It is also found that the value of $H_{c2}(0)$ is the same as that obtained from the Werthamer–Helfand–Hohenberg formula [84] if the spin paramagnetic effect and the spin–orbit interaction are taken into account by utilizing the relation $\gamma(H) \propto H$ and the value of $d\gamma/dH$ [13, 14] as discussed later. It is observed that the critical field behaviour of 60 nm thin film [20] is comparable to that of sintered $MgCNi_3$ powders. Films thicker than ∼40 nm have an upper critical field $H_{c2} \sim 13$ T, which is comparable to that of polycrystalline bulks [16, 20, 48].

The Pauli limiting field $H_P(0) = 1.84 \times 10^4 T_c$ is expected within the weak coupling BCS theory [86]. The $H_{c2}(0)$ [9] obtained from Werthamer–Helfand–Hohenberg theory [84]

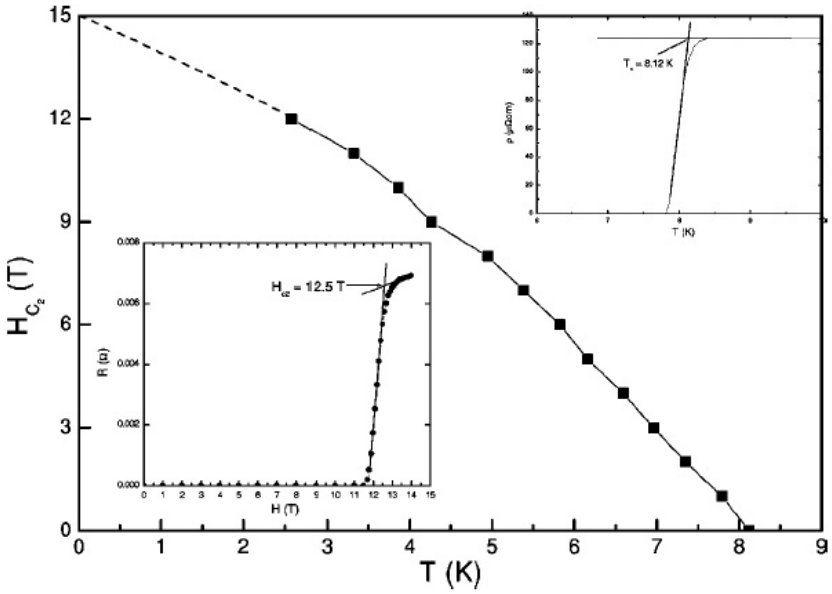

Figure 10. The upper critical field H_{c2} of $MgCNi_3$ as a function of temperature. The upper inset shows the temperature dependence of the sample resistivity at zero magnetic field. The lower inset shows the magnetic field dependence of the resistance at a temperature of 2.3 K [4].

is higher than $H_P(0)$, suggesting that pair breaking effects due to the Zeeman energy in $MgCNi_3$ are slight. For type-II superconductors, $H_P(0)$ should satisfy the relation [87] $H_{c2}(0) \leqslant H_P(0)$. Taking $T_c = 6.4$–8 K (table 3), $H_P(0)$ is estimated as ∼11.7–14.72 T. Thus $H_P(0)$ for $MgCNi_3$ is of the order of its $H_{c2}(0)$ (table 3), indicating type-II superconductivity. The thermodynamic critical field $H_c(0) \sim 0.18$–0.6 T, Ginzburg–London (GL) coherence length $\xi_{GL}(0) \sim 45$–56 Å, penetration depth $\lambda_{GL}(0) \sim 1800$–2480 Å and lower critical field $H_{c1}(0) \sim 10$–12.6 mT (table 3) are generally estimated from the following relations [88, 89]:

$$H_c(0) = 4.23\gamma_n^{1/2} T_c \text{ Oe}, \tag{7}$$

$$\xi_{GL}(0) = \{\Phi_0/[2\pi H_{c2}(0)]\}^{1/2} \text{ Å}, \tag{8}$$

$$\lambda_{GL}(0) = 6.42 \times 10^5 (\rho_{res}/T_c)^{1/2} \text{ Å}, \tag{9}$$

$$H_{c1}(0) = H_c(0)(2^{1/2}\kappa)^{-1} \ln\kappa \text{ Oe}, \tag{10}$$

where the fluxon $\Phi_0 \approx 2.0678 \times 10^9$ Oe Å^2 and $\kappa(0)$ $[=\lambda_{GL}(0)/\xi_{GL}(0)] \sim 43.3$–66. All the parameters obtained for $MgCNi_3$, $\xi_{GL}(0)$, $\lambda_{GL}(0)$ and $\kappa(0)$, also satisfy the conditions for type-II superconductivity [89].

5.2. The critical current density (J_c)

Figure 11(a) shows the critical current density (J_c) of $MgC_{1.5}Ni_3$ [11] at different temperatures (1.8–6.5 K). Assuming that the current flows through the entire sample, Cooley *et al* [11] calculate that $J_c = 3\Delta M/d$, taking the applied magnetic field perpendicular to the thin square prism, where ΔM is the full width of the magnetization and d is the width of the sample. The calculation shows that $J_c \sim 10^3$–10^4 A cm^{-2} at 4.2 K. Taking into consideration the presence of carbon in grain colonies, inferred from microstructural analysis [11], the modified J_c $(=16\Delta M/3\pi a)$, with the critical state of a sphere of diameter $2a = 10$ μm,

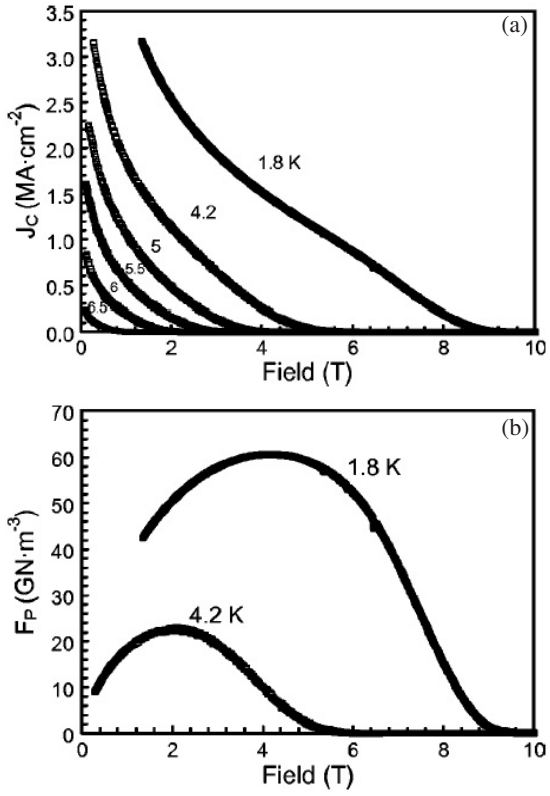

Figure 11. (a) The critical current density (J_c) at 1.8–6.5 K, assuming that magnetization current loops flow around grain colonies with diameter 10 μm. (b) The bulk pinning force (F_P) at 1.8 and 4.2 K derived from the $J_c(H)$ data using a scaling length of 10 μm colony size [11].

gives a very high $J_c \sim 1.8 \times 10^6$ A cm^{-2} at 1 T and 4.2 K. Again the pinning force, $F_P(H) = \mu_0 H \times J_c(H, T)$, derived from J_c is significantly higher for the latter assumption (figure 11(b)). The peak value is found as 23.5 GN m^{-3} at 4.2 K, which is greater than that of the Nb–48% Ti superconductor with the higher irreversibility field at 4.2 K [90]. Cooley *et al* [11] argue that the Ginzburg–Landau (GL) parameter, $\kappa(0) = 66$, of $MgCNi_3$ (table 3) suggests that the pinning force per flux line $J_c \times \phi_0 \sim 2 \times 10^{-5}$ N m^{-1} is about 10% of the flux line tension $\mu_0 H_{c2}^2 \pi \xi_{GL}/2\kappa^2 \sim 1.5 \times 10^{-4}$ N m^{-1}, taking $\phi_0 = 2 \times 10^{-15}$ Wb as the flux quantum. This strong pinning is within the single-vortex pinning regime where it plastically deforms the flux line lattice [11]. The high value of F_P at 1.8 K (figure 11(b)) suggests core pinning in $MgCNi_3$ [11]. The low field pinning characteristic can be exceeded by incorporating nanoprecipitates in $MgCNi_3$ [35]. However, too many precipitates within the grain boundaries can block uniform current flow between grains. The bulk pinning force $F_P(H)$ is comparable to that of other strong flux pinning superconductors, such as Nb–N, Nb–Ti and Nb_3Sn, all of which have higher critical temperatures [11]. While $F_P(H)$ indicates the expected grain boundary pinning mechanism just below $T_c \sim 7.2$ K, a systematic change to a core pinning mechanism is indicated by a shift of the $F_P(H)$ curve peak to higher (reduced) field with decreasing temperature. The lack of temperature scaling of $F_P(H)$ suggests the presence of pinning sites at a nanometre scale inside the grains, smaller than the diameter of the fluxon cores $2\xi_{GL}(T)$ at high temperature, which become effective when the coherence length $\xi_{GL}(T)$ approaches the nanostructural scale with decreasing temperature. It is concluded that no other fine grained bulk intermetallic superconductor exhibits a similar change from grain boundary to core pinning with decreasing temperature, suggesting that the arrangement of pinning sites in $MgCNi_3$ is

unique [11]. These results also indicate that strong flux pinning might be combined with a technologically useful upper critical field if variants of $MgCNi_3$ with higher T_c can be found.

5.3. The normal state magnetoresistance (MR)

Normal state magnetoresistance (MR) is an important tool for getting further insight into the charge transport mechanism, since it is more sensitive to the change in the charge carrier scattering rate $1/\tau$, the effective mass m^* and the geometry of the Fermi surface. The MR is given by $\Delta\rho/\rho_0 = [\rho(H) - \rho_0]/\rho_0$ where $\rho(H)$ and ρ_0 are respectively the resistivities with and without a magnetic field H. Since the charge carrier scattering rate, $1/\tau$, is proportional to ρ_0, the MR depends only on H/ρ_0. Kohler's rule for conventional superconductors is given by [91]

$$\mathrm{MR} = \Delta\rho/\rho_0 = f(H\tau) = F(H/\rho_0) \tag{11}$$

where f and F are universal functions. In the low field limit, $\Delta\rho(T) = A(H/\rho_0)^2$ as MR quadratically depends on H, where A is a constant. The resistance of $MgCNi_3$ increases with magnetic field (figure 12) showing a positive magnetoresistance [7]. It is also comparable to that of a normal metal [91]. However, the MR of $MgCNi_3$ is much smaller than that for the borocarbide superconductors [7]. It is found that the normal state transverse MR of $MgCNi_3$ is always positive and monotonically decreases with increasing temperature (figure 12). The data above 50 K follow Kohler's rule, although those below 50 K do not. This electronic crossover at 50 K is also observed in NMR data [3], which may be associated with this deviation of MR from Kohler's rule below 50 K. Here it should be mentioned that Das and Kremer [33] observe a negative MR at 2 K and followed by a $\sim H^2$ dependence for $MgCNi_{2.97}Mn_{0.03}$ samples. The authors of [33] argue that the negative MR is from partial alignment of impurity spins reducing the spin flip scattering. They [33] also show a correlation between MR and M^2 indicating the Kondo effect [92]. This can be described by the relation

$$\Delta R = R(H, T) - R(0, T) = [3\pi^2 mcVJ^2M^2]/[E_F e^2 h] \tag{12}$$

where m and e are respectively the charge and mass of an electron, V is the atomic volume, J is the s–d exchange constant, c is the atomic concentration of impurities, E_F is the Fermi energy, h is Planck's constant and M is the magnetization in μ_B/atom. ΔR versus M^2 indeed satisfies the above relation (equation (12)) for $MgCNi_{2.97}Mn_{0.03}$ samples [33].

5.4. The Hall effect

Hall effect measurements are used to get a direct idea of the type of the carriers (namely electrons or holes) in a material. They can also give the number of carriers per unit volume (n). The Hall coefficient (R_H) of $MgCNi_3$ at a magnetic field of 10 T is almost constant up to a temperature of 140 K (figure 13) and beyond that the magnitude decreases with increase of the temperature [4]. The inset of figure 13 shows the increase of the Hall voltage (V_H) measured at 100 K with increase of the magnetic field in the opposite direction. R_H of $MgCNi_3$ is negative for the whole temperature range, which definitely indicates that the carriers in $MgCNi_3$ are of electron type, as supported by the thermoelectric power data [7, 17, 39]. At $T = 100$ K, $R_H = -6.1 \times 10^{-10}$ m^3 C^{-1} and the carrier density (n) was 1.0×10^{22} cm^{-3}, which is comparable with the theoretically calculated [50] value (1.3×10^{22} cm^{-3}) and that for perovskite (Ba, K)BiO_3, but less than that for the metallic binary MgB_2. However, the value of n for $MgCNi_3$ thin film [20] is found to be 4.2×10^{22} cm^{-3} (table 3) which is about four times higher than that of the bulk sample [4] although the superconducting properties of bulk and thin film samples are almost the same. Again the R_H depends on temperature, which is not observed

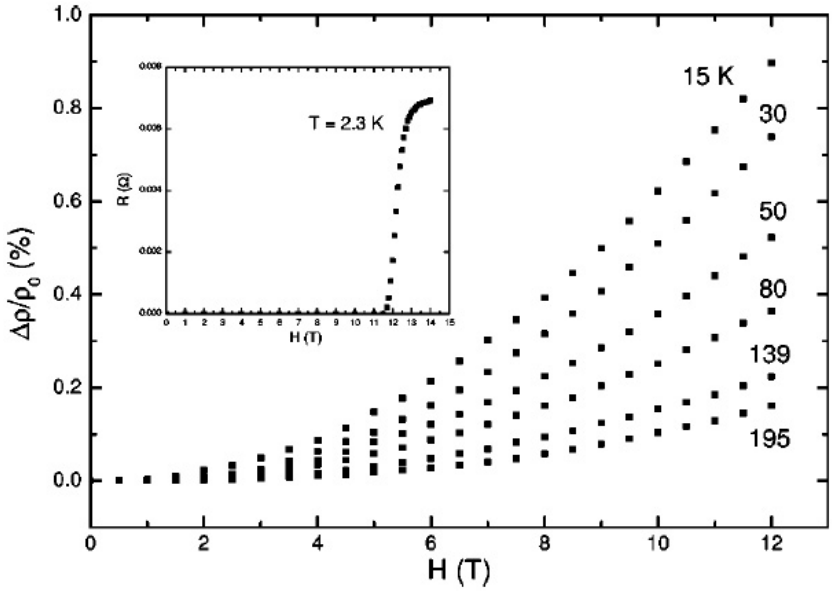

Figure 12. The magnetoresistance of $MgCNi_3$ as a function of the magnetic field at various temperatures. The inset shows the magnetic field dependence of the resistance at 2.3 K [7].

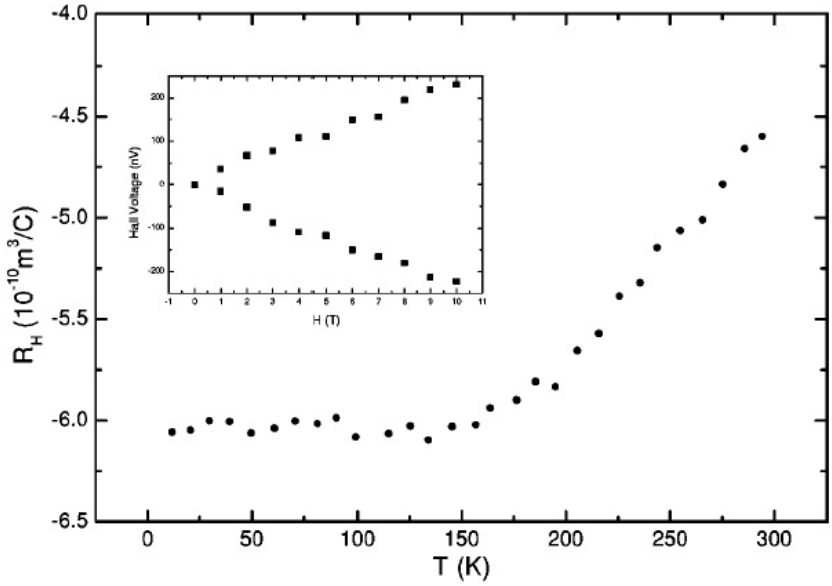

Figure 13. The temperature variation of the Hall coefficient (R_H) measured at a magnetic field of 10 T. The inset shows the Hall voltage measured at 100 K for two opposite directions of the applied field up to 10 T [4].

for conventional superconductors. Moreover, it is temperature independent between T_c and 140 K. Above 140 K, the magnitude of R_H decreases with increase of the temperature [39]. The temperature variation of R_H is also observed in non-cuprate $Ba_{1-x}K_xO_3$ and copper-based

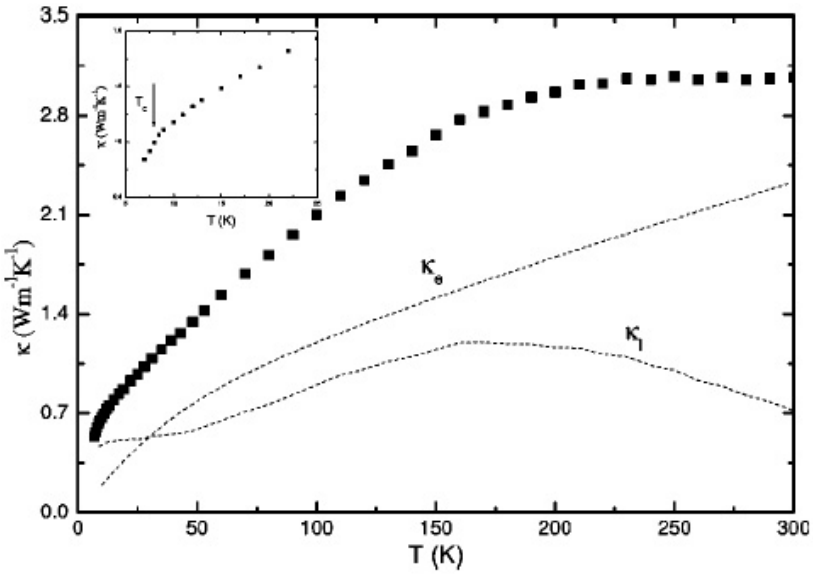

Figure 14. The temperature variation of the thermal conductivity of $MgCNi_3$. The dashed curves represent the electronic contribution k_e and the lattice contribution k_l. The inset shows the change of slope at $T_c = 8$ K [7].

superconductors [93, 94]. The thermal dependence of R_H in $MgCNi_3$ may be explained as due to magnetic excitations of the electrons supplied by Ni d states [49–54]. But interestingly the non-cuprate $Ba_{1-x}K_xO_3$ has the same temperature behaviour [93] of R_H, which needs further investigation.

6. Thermal properties

6.1. The thermal conductivity (k)

The temperature variation of the thermal conductivity (k) of $MgCNi_3$ (figure 14) shows that it is nearly constant above 210 K [7]. It is of the order of that for intermetallics, larger than that of borocarbides [95] and smaller than that of MgB_2 [96]. A change of slope in the thermal variation of k is observed at T_c (figure 14). The total thermal conductivity $k = k_e + k_l$ where k_e and k_l are respectively the electronic and lattice contributions in k. The electronic contribution can be obtained from the Wiedemann–Franz law [97]

$$k_e(T) = L_0 T/\rho(T) \tag{13}$$

where L_0 is the Lorentz number, ρ is the resistivity and T is the absolute temperature. Then the lattice contribution is achieved from the total thermal conductivity. The electrons contribute a large fraction to the thermal conductivity in the normal state because of the non-localization of the mutual effect of electrons [61]. Analysis of the electronic thermal conductivity indicates that the scattering by impurities prevails in the electronic thermal resistance. It has been observed [7] that the electronic contribution is slightly higher than the lattice contribution in the normal state (figure 14). It has also been found from thermal conductivity that the scattering of electrons by static imperfections of the crystal becomes dominant near T_c [7]. However, the spin fluctuations are increased with decrease of the temperature [3] and the scattering of electrons with spin fluctuations decreases the thermal conductivity at low temperatures.

6.2. The thermoelectric power (TEP)

The lower part of figure 4 shows the thermoelectric power (S) of the MgC_xNi_3 sample [17] with $x = 1.0$ (sample A). The temperature dependence of S is negative, confirming the carriers to be of electron type, which is consistent with other published results [4, 7, 39] and inconsistent with the theoretical predictions [50]. The absolute value of $S(275\ \mathrm{K}) \sim 9.5$–$14\ \mu\mathrm{V\ K^{-1}}$ for this sample decreases with decreasing temperature and is a characteristic of metallic transport in the normal state [7, 17]. The magnitude of S at room temperature (RT) is higher than that associated with free electron or conventional metals but of the same order as that for RNi_2B_2C (R = rare earth) superconductors [7]. There are generally diffusion and phonon drag contributions to S. The former contribution is proportional to temperature (T) while the latter one falls both at low and high temperature, respectively due to the freezing out of the phonons and phonon–phonon scattering. No phonon drag peak is observed in S of $MgCNi_3$ from room temperature down to 10 K [7]. A different type of contribution to S is found compared to the borocarbide case; it may be due to the three-dimensional (3D) and non-layered nature of $MgCNi_3$. Li *et al* [7] observe a nonlinear temperature dependence of S below 150 K, which is explained by the electron–phonon interaction renormalization effects. The nonlinear temperature dependence of S [7, 39] seems to suggest that the enhancement of the electron–phonon interaction plays an important role in the superconductivity of $MgCNi_3$ like in the chevrel phase compounds [98] $Cu_{1.8}Mo_6S_{8-y}Se_y$ and $Cu_{1.8}Mo_6S_{8-y}Te_y$. An electronic crossover occurs at about 50 K, resulting in the abnormal behaviour of S below 50 K [39].

The electron–phonon interaction renormalization effect may show a low temperature 'knee' in $S(T)$ and may be written as [98]

$$S/T = (S_b/T)[1 + \lambda(T)] \tag{14}$$

where $\lambda(T)$ is the electron–phonon mass enhancement parameter which is maximum at $T = 0$ but becomes very small near room temperature [7] and S_b is the bare S without any renormalization effect. Li *et al* [7] observe a change of curvature in the S/T versus T curve near 50 K, as is also observed by Singer *et al* [3] from NMR investigation, which may be associated with the electronic crossover at 50 K prior to the superconducting transition. Li *et al* [7] estimate the value of $\lambda(0)$ from S data as $\sim$1.4, which is much higher than that ($\sim$0.66–0.84; table 3) calculated from low temperature specific heat (C) data [1, 9, 13, 38, 47, 48] (discussed later). This suggests that there may be a mechanism other than the electron–phonon interaction for the mass enhancement. $MgCNi_3$ has a strong spin fluctuations [3, 13] which may be lessened with decreasing temperature. The larger value of $\lambda(0)$ obtained from S data compared to that obtained from C data may be arising from spin fluctuations. Thus the modified S is of the form

$$S/T = (S_b/T)[1 + \lambda(T) + \lambda_{sf}] \tag{15}$$

where λ_{sf} is the mass enhancement parameter due to spin fluctuations. The λ_{sf} term can explain the discrepancy between the values of $\lambda(0)$ obtained from S and C data [1, 3, 7, 13].

6.3. The specific heat (C)

The specific heat (C), a thermodynamic bulk property, unlike resistivity and magnetization, of $MgCNi_3$ has been intensively studied by several groups [1, 13, 24, 38, 48]. Figure 15 shows the low temperature specific heat $C(T, H)$ of $MgCNi_3$ with $H = 0$ and 8 T as C/T versus T^2 [13]. The superconducting anomaly observed by Lin *et al* [13] at $H = 0$ is much sharper than that observed by He *et al* [1], indicating the high quality of the sample of the former group. The C data are discussed on a qualitative level in terms of effective single- and

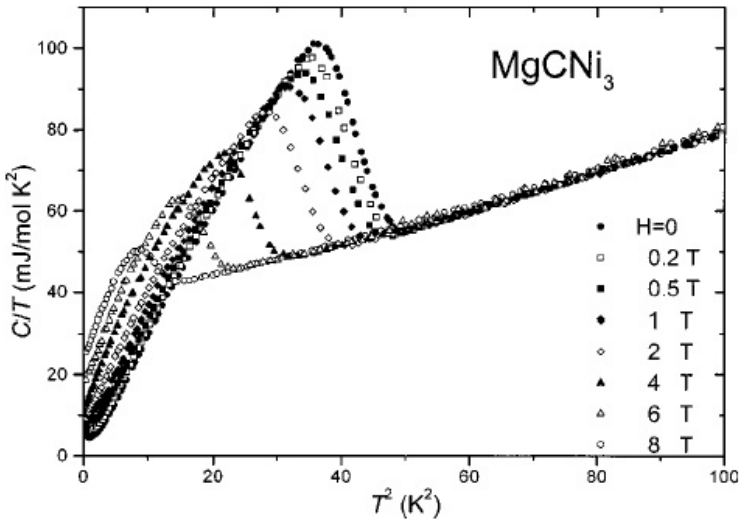

Figure 15. $C(T, H)/T$ versus T^2 for $MgCNi_3$ for $H = 0$–8 T [13].

multi-band models [24, 48] based on an orbital assignment of the disjoint Fermi surface sheets (FSS) derived from LDA full-potential electronic structure calculations. It is noted that C/T shows an upturn at very low temperatures [1, 13] and disappears in high field, which is a demonstration of a paramagnetic contribution such as a Schottky anomaly. The normal state specific heat, $C_n(T) = \gamma_n T + C_{lattice}(T)$, was extracted from $H = 8$ T data by Lin *et al* [13] between 4 and 10 K using

$$C(T, H = 8\ \mathrm{T}) = \gamma_n T + C_{lattice}(T) + nC_{Schottky}(g\ \mu H/k_B T), \tag{16}$$

where the third term is a two-level Schottky anomaly. $C_{lattice}(T) = \beta T^3 + \delta T^5$ represents the phonon contribution and $\gamma_n T$, the electronic contribution with γ_n as the coefficient of the electronic specific heat in the normal state. It was found by several groups that $\gamma_n = 9.8$–11.2 mJ K^{-2} (mol Ni)$^{-1}$ (table 3). The value of γ_n increases with increasing Mn concentration in $MgCNi_{3-z}Mn_z$ samples [33]. This observation indicates that the reduction in T_c with addition of Mn is due to the pair breaking interaction, which is of magnetic origin and not electronic [33]. This value of γ_n, with the electron–phonon coupling constant λ discussed below, requires a higher band $N(E_F)$ than most of those reported from calculations [49–51, 54–57]. It is found that for MgC_xNi_3, the γ_n of the superconducting sample ($x \sim 1$) in the normal state is twice than that of the sample in the non-superconducting state ($x \sim 0.85$) [47]. Comparison of the measured γ_n and the calculated electronic DOS shows that the effective mass renormalization changes remarkably as the carbon concentration alters. The Debye temperature (θ_D) derived from the relation

$$\beta = 1.944 \times 10^6 \times n/\theta_D^3, \tag{17}$$

where n is the number of atoms per formula unit and takes the value 5 for $MgCNi_3$, varies from 206 to 351 K (table 3) and is much lower than that (450 K) of Ni. These values are also lower than the calculated $\theta_D \sim 440$ K of $MgCNi_3$ obtained by using the Rietveld refinement method based on the powder XRD data [29]. However, these are close to that estimated by considering the softening of the Ni lattice [51], which can enhance the electron–phonon interaction. The concentration of paramagnetic centres can be estimated to be of the order of 10^{-3}, consistent with that assessed from the magnitude of the low temperature upturn. With a dominant content of Ni in this compound, this number is understandable and the paramagnetic contribution is indeed observed in the magnetization measurements, too [23].

The characteristics of the superconducting phase transition in $MgCNi_3$ can be analysed using the relation

$$\Delta C(T) = C(T, H = 0\ \mathrm{T}) - C_{\mathrm{n}}(T). \tag{18}$$

The resultant $\Delta C(T)/T$ versus T at $H = 0$ is shown in figure 16(a), where the inset illustrates the conservation of entropy $S = \int_0^{T_c} \frac{\delta C}{T}\,\mathrm{d}T$ around the transition. This conservation of entropy is essential for a second-order (such as the superconducting–normal) phase transition. It is worth noting that $\Delta C(T)/T$ for $MgCNi_3$ is qualitatively different from that of Sr_2RuO_4, which is considered as a p-wave superconductor [99]. By the conservation of entropy around the transition, the dimensionless specific heat jump at T_c is $\Delta C/\gamma_n T_c = 1.7$–$2.1$ (table 3), as shown in figure 16(b) [13], which is greater than the typical weak coupling value ($\sim$1.43). Thus $\Delta C(T)/T$ is well fitted by the BCS model, as shown in figure 16(a) by the solid curve [13] with $2\Delta/k_B T_c \sim 4.0$, where Δ is the superconducting energy gap. The values of $2\Delta/k_B T_c$ observed by different groups vary from 3.75–5.0 (table 3). This is higher than the weak coupling value ($\sim$3.52). Consequently, the superconductivity in $MgCNi_3$ can be explained by the moderate coupling BCS framework.

The electronic specific heat in the superconducting state is given by $C_{\mathrm{es}}(T) = C(T) - C_{\mathrm{lattice}}(T)$. A logarithmic plot of $C_{\mathrm{es}}(T)/\gamma_n T_c$ versus T_c/T (figure 17) shows that the fitting of data (as demonstrated by the solid line) within the range 2 to 4.5 K leads to [13] the relation

$$C_{\mathrm{es}}(T)/\gamma_n T_c = A \exp[(-aT_c/T)], \tag{19}$$

with $A = 7.96$ and $a = 1.46$. However, the BCS theory predicts $C_{\mathrm{es}}(T)/\gamma_n T_c = 8.5 \times \exp[(-1.44T_c/T)]$ for this temperature fitting range in the weak coupling limit [80]. Therefore, the values of both the coefficient and the prefactor are in the ranges for typical moderate coupling BCS fully gapped superconductors. Lin *et al* [13] argue that since the magnetic contribution will make C_{es} overestimated at low temperatures, the value of 1.46 in the exponent is probably slightly underestimated. This is in contrast to the case for MgB_2 [100], for which $C_{\mathrm{es}} \propto \exp(-0.38T_c/T)$. This small coefficient in the exponent for MgB_2 is usually attributed to a multi-gap order parameter.

The electron–phonon coupling constant $\lambda \sim 0.66$–0.84 (table 3) is estimated from the relation [101]

$$\Delta C/\gamma_n T_c = 1.43 + 0.942\lambda^2 - 0.195\lambda^3. \tag{20}$$

According to McMillan model [80], the value of λ for weak coupling is $\lambda \ll 1$, for weak and intermediate coupling $\lambda < 1$ and for strong coupling $\lambda > 1$. Therefore, the present λ values suggest that $MgCNi_3$ is a moderate coupling superconductor.

The field dependences of $C(T, H)/T$ and $\delta C(T, H)$ ($\equiv C(T, H) - C_{\mathrm{n}}(T))/T$ are shown in figures 18(a) and (b), respectively. It is noticed that the conservation of entropy (the areas above and below zero of C/T are equivalent around the superconducting transition) is fundamentally satisfied for all fields studied. $\gamma(H)$ is expected to be proportional to H for a gapped superconductor [102]. For nodal superconductivity, the relation between $\gamma(H)$ and H is expected to be $\gamma(H) \propto H^{1/2}$ [103]. Actually, $\gamma(H)$ for high temperature cuprate superconductors has been intensively studied in this context [103, 104]. Lin *et al* [13] find that $\gamma(H)$ follows a straight line passing through the origin, which suggests that $\delta\gamma \propto H$. At $T = 2$ K, the magnetic contribution is not so significant as that at 0.6 K; thus [105, 106]

$$C_{\mathrm{es}}(T, H) \approx C_{\mathrm{es}}(T, H = 0) + \gamma(H)T. \tag{21}$$

This approximation neglects the temperature dependence of Δ. However, since Δ varies slowly below $T_c/2$, information on $\gamma(H)$ can still be deduced in this way consistently, as we will see from $\mathrm{d}\gamma/\mathrm{d}H$. $\delta C/T$ data for all fields are shown as the solid circles (figure 18). As seen in

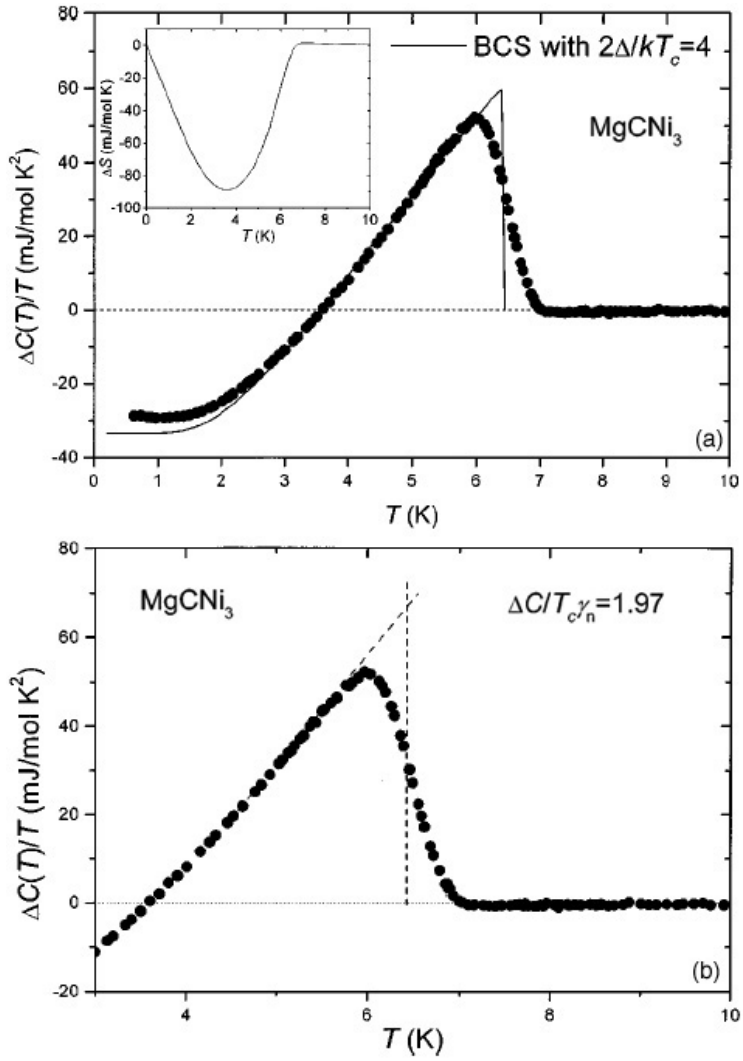

Figure 16. (a) $\Delta C(T)/T$ versus T. The data are presented as the solid circles. The solid curve is the BCS $\Delta C(T)/T$ with $2\Delta/kT_c = 4$. The deviation at low temperatures from the solid curve is due to the magnetic contribution of a small amount of paramagnetic centres in the sample. Inset: the entropy difference ΔS obtained by integration of $\Delta C(T)/T$ according to the data above 3 K and the solid curve below 3 K. (b) The dashed lines are determined from the conservation of entropy around the anomaly, to estimate $\Delta C/T_c$ at T_c [13].

figure 18(b), all high field data can be well described by the straight line, indicating again a linear H dependence of γ [13]. Data below $H = 1$ T begin to deviate from the linear behaviour due to flux line interactions at low H, as nicely demonstrated in [106]. The straight line passes through the origin in figure 18(a), which implies that the flux line interactions are relatively insignificant compared to the core contribution at very low temperatures. This trend is also observed in [106]. The slopes $d\gamma/dH$ in figures 18(a) and (b) are 2.91 ± 0.05 and 3.15 ± 0.08 mJ mol^{-1} K^{-2} T^{-1}, respectively. These two close values derived from different methods suggest that the relation $\delta\gamma \propto H$ is genuine [13]. On the other hand, one may try to fit the data in figure 18(b) with

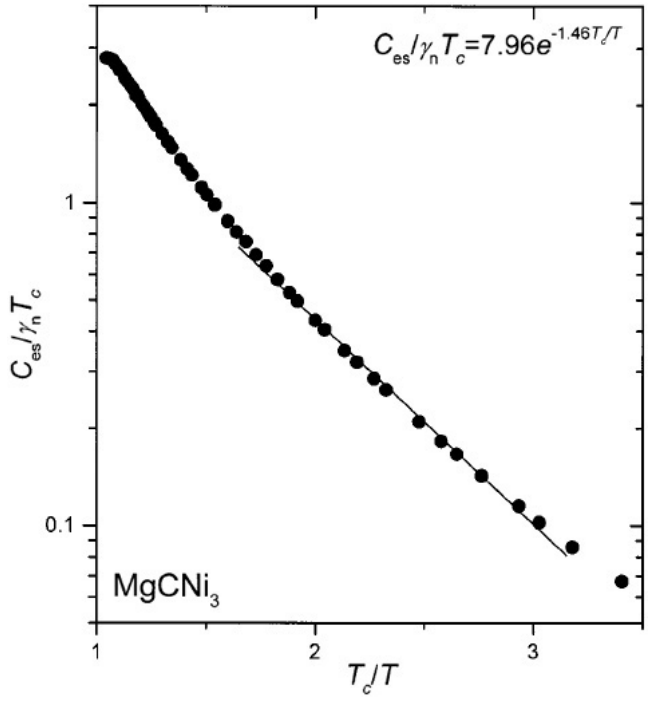

Figure 17. C_{es} for $MgCNi_3$ in the superconducting state is plotted on a logarithmic scale versus T_c/T. The straight line is the fit from 2–4.5 K [13].

$\delta\gamma(H) \propto H^{1/2}$. The results are represented by the dashed curve in figure 18(b). Apparently, the data cannot be well described in this manner, in contrast to the nice $\delta\gamma(H) \propto H^{1/2}$ relation found for cuprates [107, 108]. In principle, it is possible to obtain $\gamma(H)$ in low fields by subtracting the paramagnetic contribution $C_m(T, H)$ from $C(T, H)$. There have been attempts to obtain $\gamma(H)$ by taking $C_m(T, H)$ in the form of a Schottky anomaly [13, 22]. It is found that the derived $\gamma(H)$ can differ depending on the details of the fitting. This implies that the Schottky anomaly cannot totally account for the magnetic contribution at low temperatures. The results are fascinating but inconclusive [13, 22]. Consequently, the field dependence of $\gamma(H)$ suggests that $MgCNi_3$ is an s-wave superconductor in nature.

7. Mechanical properties

The mechanical relaxation properties of $MgC_{1-x}Ni_3$ with $x = 0$ (superconducting) and 0.2 (non-superconducting) were measured by Yao *et al* [40]. The internal friction (Q) and modulus (Y) of the mechanical relaxation spectra were measured for rectangular bars in the clamped–free flexural vibration mode using frequency modulation acoustic attenuation (FMAA-I) equipment [40]. The schematic set-up of the equipment is shown in the inset of figure 19. The mechanical relaxation spectra of a superconducting $MgCNi_3$ sample show two internal friction peaks (at 300 K labelled as P1 and 125 K, as P2) as shown in figure 19, whereas for the non-superconducting one, the position of P1 shifts to 250 K, while P2 is almost completely depressed [40]. Thus the peak P2 may be thermally activated. It is found from the Arrhenius relation

$$2\pi f_p = \nu_0 \exp(-W/T_p) \tag{22}$$

where f_p is the resonant frequency, T_p is the peak temperature and $\nu_0 = 2.9 \times 10^9$ Hz that the value of the activation energy (W) is 0.13 eV. It is observed that the peak position

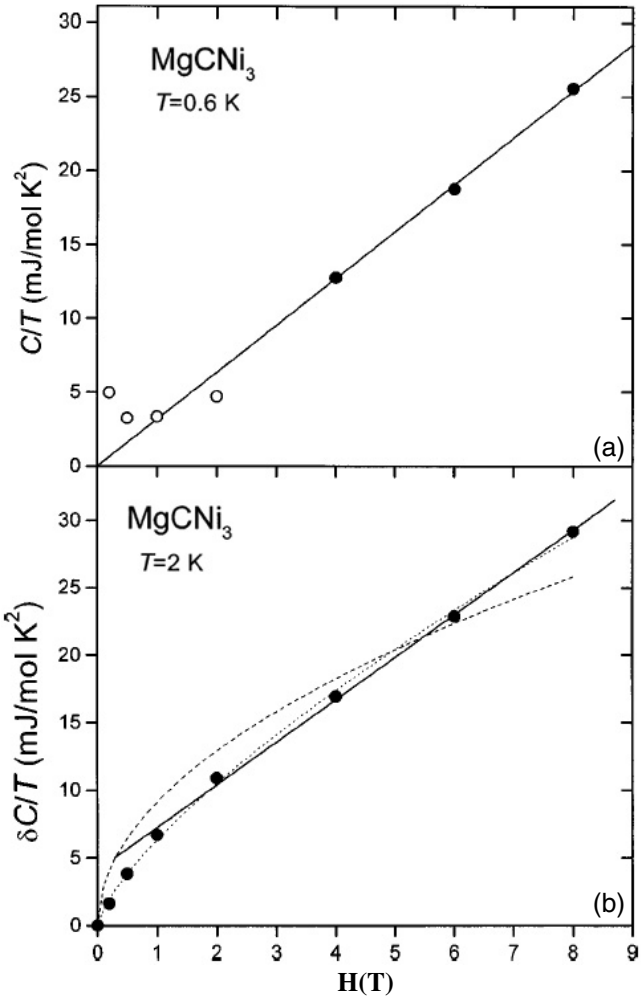

Figure 18. The magnetic field dependence of (a) C/T at $T = 0.6$ K and (b) $\delta C/T$ at $T = 2$ K. The straight lines are linear fits of the data for $H \geqslant 4$ T, implying $\delta\gamma \propto H$. The open circles in (a) represent C/T data corrected with the Schottky term (see the text). In (b), the fitting range is from 1 to 8 T. Data below $H = 1$ T deviate from the linear behaviour due to flux line interactions at low H. The fits with $\delta\gamma(H) \propto H^{1/2}$ and $\delta\gamma(H) \propto H^n$ are also shown, by the dashed and dotted curves, respectively, in (b) for comparison. The latter leads to $n = 0.73$ [13].

of P2 shifts towards higher temperature for higher measuring frequency [40]. The relative changes of the modulus $(\Delta Y/Y)$ for the two samples are also shown in figure 19, where $\Delta Y/Y = (f^2 - f_0^2)/f^2$ with f the resonant frequency and f_0 the resonant frequency at 81 K. No clear softening (local minimum) is observed (figure 19), confirming that there is no lattice instability, and this is supported by XRD data [5] which show that the lattice parameter and the Debye–Waller factors for individual atoms decrease smoothly with decreasing temperature, and no unusual change of the structure parameters occurs near T_c. It is to be noted here that although the structure of $MgCNi_3$ is similar to that of $Ba_{1-x}K_xBiO_3$ [1], the latter has a lattice instability [40]. The prediction of Debye theory for the inverse internal friction (Q^{-1}),

$$Q^{-1} = \Delta\omega\tau/T(1 + \omega^2\tau^2), \tag{23}$$

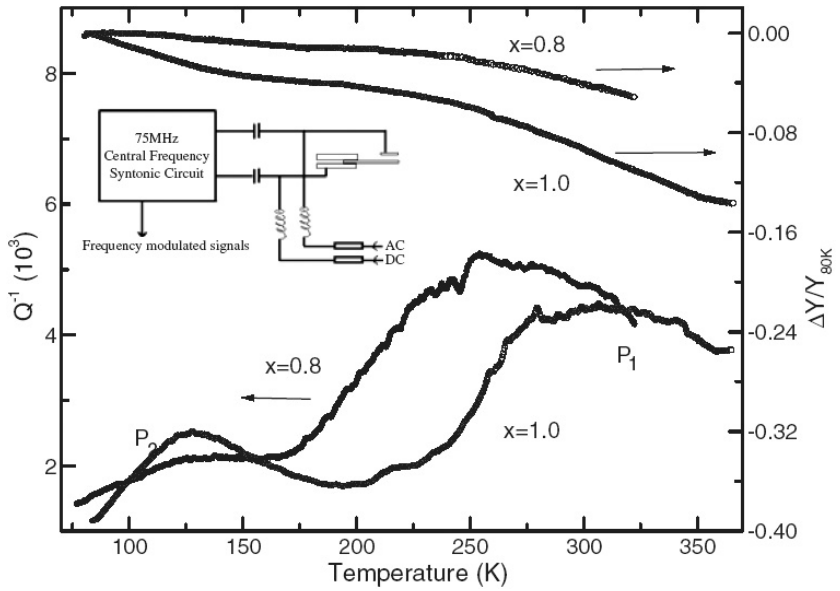

Figure 19. The inverse internal friction (Q^{-1}) and reduced modulus ($\Delta Y/Y_{80\,\mathrm{K}}$) of the mechanical relaxation spectra of the superconducting and non-superconducting $MgC_{1-x}Ni_3$ samples in the temperature range 77–300 K. The inset shows a schematic plot of the frequency modulation acoustic attenuation (FMAA-I) equipment [40].

is compared with the P2 peak, where Δ is the relaxation strength, $\omega = 2\pi f$ and $\tau = \nu^{-1}\exp(W/T_\mathrm{p})$. It is found that the prediction is much narrower than the experimental findings [40]. Thus the Cole–Cole law [109]

$$Q^{-1} = (\Delta/T)\,\mathrm{Im}[1/(1+\{\mathrm{i}\omega\tau\}^{\alpha})] \tag{24}$$

is used to fit the experimental data. It is found that $\alpha = 0.52$, indicating the existence of a strong correlation between the relaxation units. There are generally two phases in $MgC_{1-x}Ni_3$, namely non-superconducting α-$MgC_{1-x}Ni_3$ and superconducting β-$MgC_{1-x}Ni_3$ phases [28]. Due to the smaller lattice parameters of the α-$MgC_{1-x}Ni_3$ phase, the off-centre configurations would be suppressed, which is consistent with the depression of the P2 peak for the non-superconducting sample. Yao *et al* [40] propose an explanation relating P2 to carbon atom jumping among the off-centre positions. And further they predict that the behaviour of carbon atoms may correspond to the normal state crossovers around 150 and 50 K observed by many other experimental findings [3, 4, 7, 39].

8. The energy gap of $MgCNi_3$ and the type of superconductivity

Unlike the case for the MgB_2 superconductor which shows two energy gaps [100, 110], a clear gap feature corresponding to the bulk phase T_c is observed for $MgCNi_3$ [9, 19]. The superconducting energy gap Δ is found to be ∼1.5 meV by Mao *et al* [9] and ∼1.1–1.15 meV by Kinoda *et al* [19], from the tunnelling spectra of $MgCNi_3$. These values of Δ are found to be consistent with the one calculated from the specific heat and other data (table 3). The tunnelling spectroscopy and specific heat studies show that $2\Delta/k_\mathrm{B}T_\mathrm{c}$ for $MgCNi_3$ varies from 3.75 to 5 (table 3), which is higher than the typical weak coupling BCS value (∼3.52) as discussed earlier. The electron–phonon coupling constant $\lambda = 0.66$–0.84 (table 3) indicates

moderate coupling superconductivity in $MgCNi_3$. The values of the Ginzburg–London (GL) coherence length $\xi_{GL}(0) \sim 45$–56 Å, penetration depth $\lambda_{GL}(0) \sim 1800$–$2480$ Å and $\kappa(0)$ $(=\lambda_{GL}(0)/\xi_{GL}(0)) \sim 43.3$–$66$ (table 3) argue for type-II superconductivity [89] in it. Thus, from the above discussions, it can be concluded that $MgCNi_3$ is a BCS s-wave, moderate coupling, type-II, single-gap superconductor. However, this is still controversial as discussed below.

The electron tunnelling spectroscopy results and theoretically estimated superconducting parameters support a BCS s-wave pairing in $MgCNi_3$ in the weak coupling regime [19, 43, 49, 51]. The nuclear spin–lattice relaxation rate $(1/T_1)$ displays behaviour typical of isotropic s-wave superconductivity [3] with a coherence peak below T_c. The properties of Ag diffused Ag–$MgCNi_3$ and Zn doped $(Mg_{0.85}Zn_{0.15})CNi_3$ can be interpreted properly via the conventional BCS phonon mechanism [21, 41]. The difference between the low temperature specific heats of isostructural $MgCNi_3$ and $ZnCNi_3$ with similar carrier densities can be understood within the BCS framework [38].

Waelte *et al* [48] derive $\lambda = 0.84$ from the McMillan formula [80] (equation (3)), although the specific heat data show $\lambda \sim 1.45$ which is identical to the value $\sim$1.75 calculated by Ignatov *et al* [66]. Therefore, Waelte *et al* [48] conclude that strong electron–phonon coupling is present in $MgCNi_3$, which is supported by Tan *et al* [65]. The s- and p-wave scenarios are observed from the calculated DOS of different Fermi surface sheets [48]. The large mass renormalization for the superconducting sample and the low T_c ($\sim$7 K) indicate that more than one kind of boson mediated electron–electron interaction exists in MgC_xNi_3 [47]. The penetration depth exhibits distinctly a non-s-wave BCS low temperature behaviour, instead of showing quadratic temperature dependence, suggestive of a nodal order parameter [42]. Mao *et al* [9] interpret the observed zero-bias conductance peak (ZBCP) as caused by Andreev bound states which result from a possible unconventional non-s-wave pairing state in $MgCNi_3$. On this basis, of the simultaneous appearance of two conductance dips, they suggest strong coupling superconductivity in $MgCNi_3$. However, Naidyuk [45] shows that the current transport through these junctions is determined by thermal effects due to the huge normal state resistivity of $MgCNi_3$. Therefore no conclusion can be drawn about the possible unconventional pairing or strong coupling superconductivity in $MgCNi_3$ [45]. Again, Mao *et al* [46] argue, on the basis of specific heat rather than tunnelling data, that strong coupling superconductivity is suggested. Here it should be mentioned that comparing only $2\Delta/k_BT_c \sim 4.4$ with the weak coupling value of 3.52, Mao *et al* [9] suggest that $MgCNi_3$ is a strong coupling superconductor although another criterion for it, i.e. $\lambda > 1$ [80], is not satisfied.

9. Theoretical studies

The theoretical calculations on doped and undoped $MgCNi_3$ were performed by different methods as discussed below. Some of the important theoretically calculated parameters such as ΔE $(=E_{FM} - E_{PM})$, where E_{FM} and E_{PM} are respectively the energies of the ferromagnetic and paramagnetic states, the DOS at the Fermi level $N(E_F)$ and the magnetization (M) of pure and doped $MgCNi_3$ are shown in table 6. The DOS of the components of $MgCNi_3$ along with the total DOS [49] are displayed in figure 20. The electronic density of states, $N(E)$, of $MgCNi_3$ calculated within the local density approximation (LDA), along with the d contribution inside the Ni spheres, via the radius 2.04 a_0 obtained by the general potential linearized augmented plane wave (LAPW) method [50], is demonstrated in figure 21. The lower panel of figure 21 is an expanded view near the Fermi level, E_F. It is found that the band structure is dominated by a Ni 3d-derived DOS peak [49, 50] just below the Fermi energy (figures 20 and 21). The $N(E_F)$ of pure $MgCNi_3$ varies from 1.8 to 5.34 states eV^{-1}/fu (table 6). This variation in $N(E_F)$

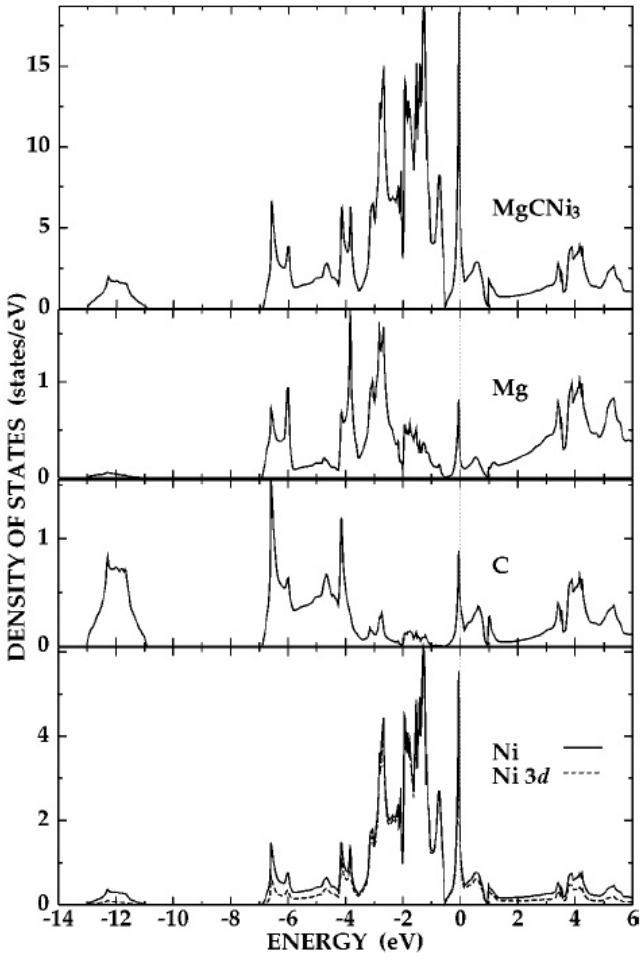

Figure 20. The total and atomic site-projected densities of states (DOS) of $MgCNi_3$ [49].

may arise from the different approximations made by different groups [49, 52, 53, 56, 57]. The linearized muffin-tin orbital (LMTO) method [51], the self-consistent spin-polarized full-potential linear muffin-tin orbital (FP-LMTO) method [53] and the self-consistent tight-binding linear muffin-tin orbital (TB-LMTO) method [52] also show that the E_F for $MgCNi_3$ is located in the slope descending from a sharp peak originating from Ni 3d states. This leads to a moderate Stoner enhancement, placing $MgCNi_3$ in the range where spin fluctuations may noticeably affect the transport, specific heat and superconductivity, providing a mechanism for reconciling various measures of the electron phonon (e–ph) coupling constant λ. Strong e–ph interactions are found for the octahedral rotation mode and may exist for other bond angle bending modes. Several other groups [51–53, 56, 58, 64] indicate that the DOS peak just below the Fermi level provides the superconducting properties of this compound. Wan *et al* [64] argue that the DOS peak is strongly correlated with various instabilities. After including the strong electron–electron (e–e) correlation effects on the Ni 3d state via the on-site Coulomb interaction correction, the DOS is greatly redistributed and the peak just below E_F disappears [64]. Shim *et al* [49] accomplish a correspondence of the peak to the π^* antibonding states of Ni 3d and C 2p but with a predominant Ni 3d character. The results calculated from density functional theory and the LDA also show that the conduction bands in this compound are derived from

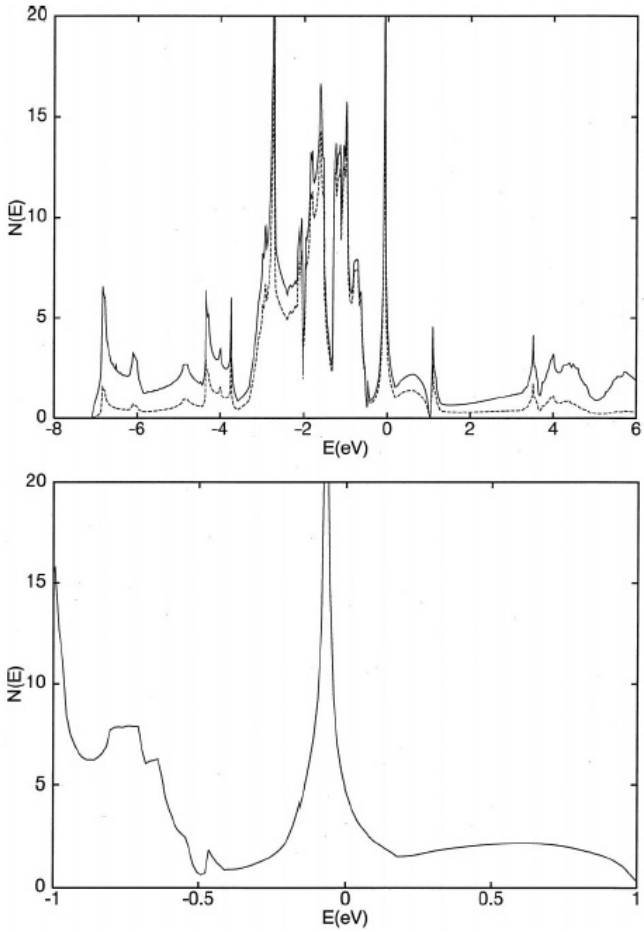

Figure 21. The electronic density of states, $N(E)$, of $MgCNi_3$ calculated within the local density approximation (upper limit). The dashed curve is the d contribution within the Ni spheres with radius 2.04 a_0 obtained by the general potential linearized augmented plane wave (LAPW) method. The lower panel is an expanded view near the Fermi level, E_F [50].

Ni 3d and C 2p states [65]. Tan *et al* [67] also find that the conduction bands in this compound are derived from Ni 3d and C 2p states. The top valence states have essentially Ni 3d character and the C 2p states occupy the region from 4.0 to 7.0 eV below the Fermi energy. The E_F locates just at the slope step of the sharply structured Ni $3d_{yz+zx}$ and $3d_{3z^2-r^2}$ peaks. Optical conductivity in the energy range 0–12 eV is also contributed by the Ni 3d to Ni 4s and C 2p transitions [65]. The optical properties of $MgCNi_3$ have been calculated using the full-potential linearized augmented plane wave (FLAPW) method within the generalized gradient approximation scheme for the exchange–correlation potential [68]. The dielectric function, reflectivity, optical absorption coefficient, optical conductivity, energy loss function, refractive index and extinction coefficient are calculated [68] to fully elucidate the optical properties of $MgCNi_3$. The calculation [68] predicts a large reflectivity and small extinction coefficient in the low energy region, as shown in figure 22. The absorption coefficient and optical conductivity are very small at low energy [68]. All these computed results need experimental verification. Wan *et al* [64] find that $MgCNi_3$ is a metal from electronic structure calculations using the local

Table 6. Some important theoretically calculated parameters for pure and doped $MgCNi_3$. Here $\Delta E = E_{FM} - E_{PM}$; E_{FM} and E_{PM} are respectively the energies of the ferromagnetic and paramagnetic states. M is the magnetization and $N(E_F)$ is in states eV^{-1}/fu.

	Parameters				
Composition	ΔE (meV)	$N(E_F)$	M (μ_B)	Model used[a]	References
$MgCNi_3$	0.2	1.8	—	FLAPW	[57]
$MgCNi_3$	—	5.34	—	LDA-LMTO	[49]
$MgCNi_3$	—	5.26	—	TB-LMTO	[52]
$MgCNi_3$	—	4.65	—	FP-LMTO	[53, 56]
$MgCNi_3$	—	4.99	—	LAPW	[53]
$MgCNi_2Co$	0.2	1.2	—	FLAPW	[57]
$MgCNi_2Co$	—	3.65	—	FP-LMTO	[56]
$MgCNiCo_2$	0.0	0.7	—	FLAPW	[57]
$MgCNi_2Fe$	0.0	0.5	—	FLAPW	[57]
$MgCNiFe_2$	−271.6	2.9	0.08(Ni)	FLAPW	[57]
MgC(FeCoNi)	−60.6	2.6	0.97(Fe)	FLAPW	[57]
$MgCNi_{2.84}Co_{0.16}$	−1.0	4.6	0.646(Co)	LDA	[58]
$MgCNi_{2.92}Co_{0.083}$	−1.8	6.5	0.638(Co)	LDA	[58]
$MgCNi_{2.95}Mn_{0.042}$	—	—	1.06(Mn)	TB-LMTO	[58]
$MgCCo_3$	−30.4	2.0	0.39(Co)	FLAPW	[57]
$MgCFe_3$	−379.1	3.4	1.42(Fe)	FLAPW	[57]
$MgBNi_3$	—	4.79	—	LDA-LMTO	[49]
$MgNNi_3$	—	3.63	—	LDA-LMTO	[49]
$ScBNi_3$	—	2.59	—	FP-LMTO	[53]
$InBNi_3$	—	1.47	—	FP-LMTO	[53]

[a] The abbreviations for the models are explained in section 9.

spin density approximation (LSDA) of the density functional theory, using the self-consistent FLAPW method. The magnetic moment on the Ni ion is only 0.014 μ_B. The magnetic moment on the Ni ion increases when electron–electron (e–e) correlation effects are considered and becomes 0.66 μ_B [64]. The ΔE of pure $MgCNi_3$ is ∼0.2 meV (table 6). It is observed that the Fermi surface contains nearly cancelling hole and electron sheets [52] that give an unusual behaviour of transport quantities, particularly the thermoelectric power. The prominent nesting feature is observed in the Γ-centred electron Fermi surface of an octahedral cage-like shape that originates from the 19th band [50].

Ignatov *et al* [66] have calculated a large coupling constant $\lambda = 1.75$ which is much higher than the experimentally observed values, ∼0.66–0.84 (table 3), but comparable to those (∼1.4–1.45) obtained by others [7, 48]. The theoretical Sommerfeld constant $\gamma_{cal} \sim 4.45$ mJ K^{-2} (mol Ni)$^{-1}$ [66] is lower than the experimental values ∼9.8–11.2 mJ K^{-2} (mol Ni)$^{-1}$ (table 3). On the basis of BCS strong coupling theory and first-principles calculation, the Debye frequency (ω_D) for $MgCNi_3$ is estimated to be 87 cm^{-1} approximately.

The surface electronic structures of $MgCNi_3(001)$ with both MgNi terminated and CNi terminated surfaces are investigated using the all-electron FLAPW method within the generalized gradient approximation to density functional theory [55]. It is found that the calculated work function of the MgNi terminated surface (∼4.17 eV) is lower than that of the CNi terminated surface (∼5.16 eV). The total numbers of electrons in the surface layer of the MgNi terminated surface and the CNi terminated surface are respectively greatly and slightly reduced with respect to the centre layer values [55]. The number of Ni(S) d electrons

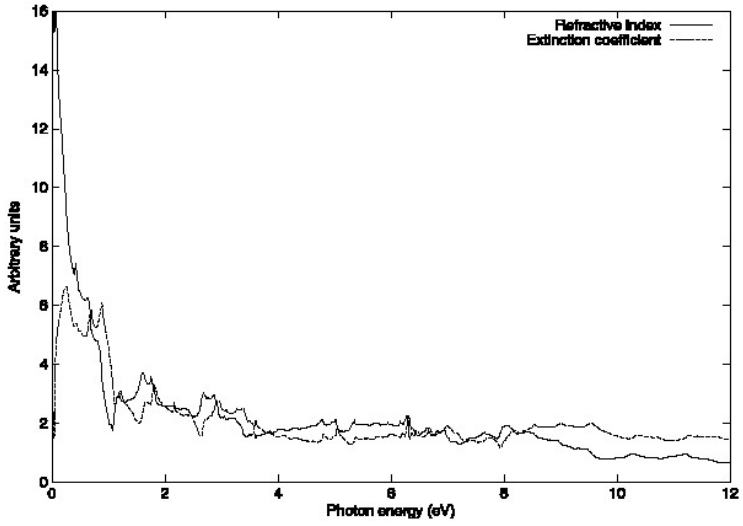

Figure 22. The calculated refractive index and extinction coefficient of $MgCNi_3$ [68].

for the MgNi terminated surface is calculated to be 0.08 electrons more than that for the CNi terminated surface. The layer-projected l-decomposed local DOS shows that the difference in the number of Ni(S) d electrons is due to the strong C p and Ni d hybridization at the surface layer of the CNi terminated surface. The peak just below E_F for bulk $MgCNi_3$ is broadened substantially at the Ni(S) CNi terminated surface, while that peak survives at the Ni(S) MgNi terminated surface [55]. By analysing the charge density for a very narrow energy window just below E_F, such considerable modifications of the DOS peak at the CNi terminated surface are distinguished as being due to the broken local symmetry of the CNi layer at the surface [55]. It is considered that the behaviour of the modification of the peak near E_F resembles the p band hole doping through C site substitution and this is supported by the stability against ferromagnetism determined from total-energy calculations [55].

The possibility of superconductivity is discussed for the intermetallics $ScBNi_3$, $InBNi_3$, $MgCCo_3$ and $MgCCu_3$ which are isostructural with $MgCNi_3$ [49]. Electronic structures of the $MgCNi_{3-z}M_z$ (M = Co, Cu; $z = 0, 0.5, 1.0$) system have been calculated using the TB-LMTO method [52]. Electron (Cu) and hole (Co) doping of $MgCNi_3$ reconstructs its band structure but does not lead to magnetic order, although the DOS initially increases with increase of the Co concentration (figure 23). However, investigation of the electronic structures and magnetism of $MgCNi_{3-z}T_z$ compounds ($z = 0, 1, 2$ and 3; T = Co and Fe) via first-principles all-electron FLAPW calculations within the local spin density approximation reveals that the suppression of superconductivity occurs faster for the Fe doped case than for the Co doped one with increase of z and ferromagnetic transitions occur when $z \geqslant 2$ for the Co doped cases, while the Fe doped cases become ferromagnetic before $z = 2$ [47]. From the calculated DOS, it is found that $MgCNi_3$ becomes paramagnetic and then ferromagnetic as the number of minority spin d band holes are increased via Co and Fe doping at Ni sites. The effects on the electronic structure and magnetic properties of the Ni site substitution in $MgCNi_{3-z}Co_z$ are studied by using density functional calculations [58]. Co doping results in the onset of ferromagnetism at $z = 0.083$. However, the slightly energy gain as well as small magnetic moment per atom indicate weak itinerant ferromagnetism [58]. Cu doping can be well accounted for by the rigid band model, which reduces the DOS at the Fermi level and the T_c [58]. Co doping of $MgCNi_3$ is accompanied by a reduction of the DOS at the Fermi level, which seems to be responsible for the reduced superconductivity in the $MgCNi_{1-z}Co_z$ system [56]. No magnetic solution is

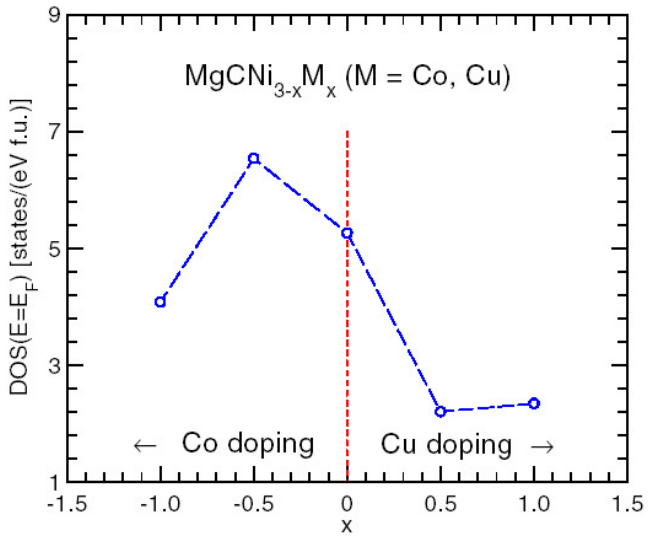

Figure 23. The density of states (DOS) at $E = E_F$ for $MgCNi_{3-x}M_x$ (M = Co, Cu) plotted as a function of the impurity concentration, x [52].

(This figure is in colour only in the electronic version)

found for $MgCNi_2Co$ and $MgCNiCo_2$ [56]. This indicates that hole doping does not produce the magnetic instability which could be responsible for pair breaking [56]. Starting from a first-principles electronic structure calculation for $MgCNi_3$ and using a simple Hartree–Fock approximation, Granada *et al* [59] compute the magnetic moment of transition impurities T in the dilute limit of $MgC(Ni_{1-z}T_z)_3$ with T = Co, Fe, Mn, Cr and V. The computation shows that Co impurities are non-magnetic and for the remaining ones at least a small moment exists. Rosner *et al* [54] observe an unusual quasi-two-dimensional heavy band mass von Hove singularity (vHs) very near the Fermi energy for $MgCNi_3$. It is pointed out [54] that this compound is strongly exchange enhanced and unstable against ferromagnetism upon hole doping with ∼12% Mg → Na or Li (i.e., 0.04 hole/Ni). An essentially infinite mass along the M–Γ line accounts for the two dimensionality of this vHs [54]. Thus this compound provides new opportunities to probe the ferromagnetic critical point as well as introducing the novelties of 2D behaviour into a 3D system. It is concluded that experimental studies on the change of T_c with concentration might indicate, for non-magnetic impurities, a d-wave behaviour of these superconductors [59].

Replacement of C by B or N greatly reduces the DOS peak [49] near E_F (figure 24). The $N(E_F)$ of $MgBNi_3$ (∼4.79 states eV^{-1}/fu) is much higher than that (∼3.63 states eV^{-1}/fu) of $MgNNi_3$ (table 6). The replacement of Mg in $MgBNi_3$ by In or Sc reduces the $N(E_F)$ even more (table 6). The total or partial replacement of Ni in $MgCNi_3$ by Co or Fe also greatly diminishes $N(E_F)$, as shown in table 6, except for $MgCNi_{2.92}Co_{0.083}$ where a higher value (∼6.5 states eV^{-1}/fu) is obtained. The magnetic moment (M) of doped $MgCNi_3$ calculated by several groups is shown in table 6. Depending on the doping element, i.e. Co, Fe, Mn etc, the value of M differs. ΔE for some doped and undoped $MgCNi_3$ samples is shown in table 6. A hypothetical system, MgC(FeCoNi), has been found to be ferromagnetic with magnetic moments of 0.97, 0.24 and 0.03 μ_B for Fe, Co and Ni, respectively; these are roughly proportional to the number of d band holes of minority spin (table 6). The role of the transition metal dopants [57] in the magnetism may be understood from the site-projected spin-polarized

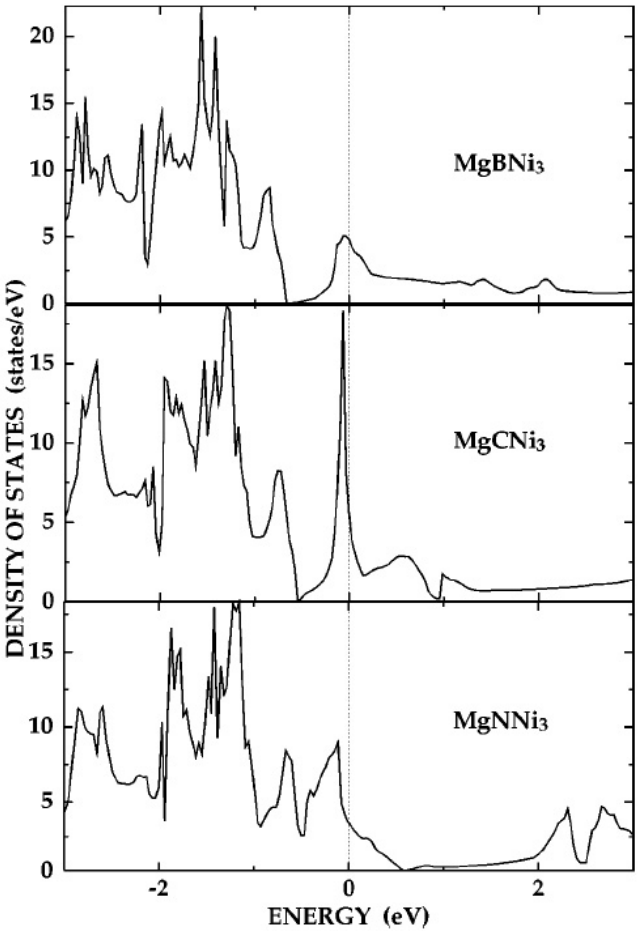

Figure 24. The density of states of $MgXNi_3$ (X = B, C, N) [49].

DOS of hypothetical MgC(FeCoNi). The majority spin d bands are seen to be nearly filled for all transition metal atoms. On the other hand, the location of E_F is shifted to the top of the minority spin d band as we move from Fe to Ni, which is again understood as behaviour typical of metallic ferromagnetism. It also confirms that Co and Fe doping in $MgCNi_3$ provide a source of minority spin d band holes rather than magnetic scattering centres that quench superconductivity. In addition, their locations and the widths of the main peaks of the minority spin d bands are seen to be rather independent of each other, but the shape of the Fe d bands is modified from that in the bcc phase [57]. This again confirms the independence of the magnetic moments of the face centred transition metal atoms. The strong ferromagnetic spin fluctuation in $MgCNi_{3-z}Co_z$ leads to quenched bulk superconductivity, while the Mn atom forms a local magnetic moment of 1.06 μ_B at $z = 0.042$ which suppresses superconductivity more seriously than Co does in the low doping case [58]. There is a large variation of ΔE (−379.1–0.2 meV) according to the difference in composition.

A two-band model [18, 24, 48] provides a consistent interpretation of the temperature dependence of the normal state resistance and the Hall constant. The thermoelectric power also needs to be explained by a multi-band model [48]. Although the band structure calculations suggest an increase in T_c upon partial replacement of Ni with Fe and Co, the Co substitution quenches the superconductivity and Fe substitution leads to an increase followed by a decrease

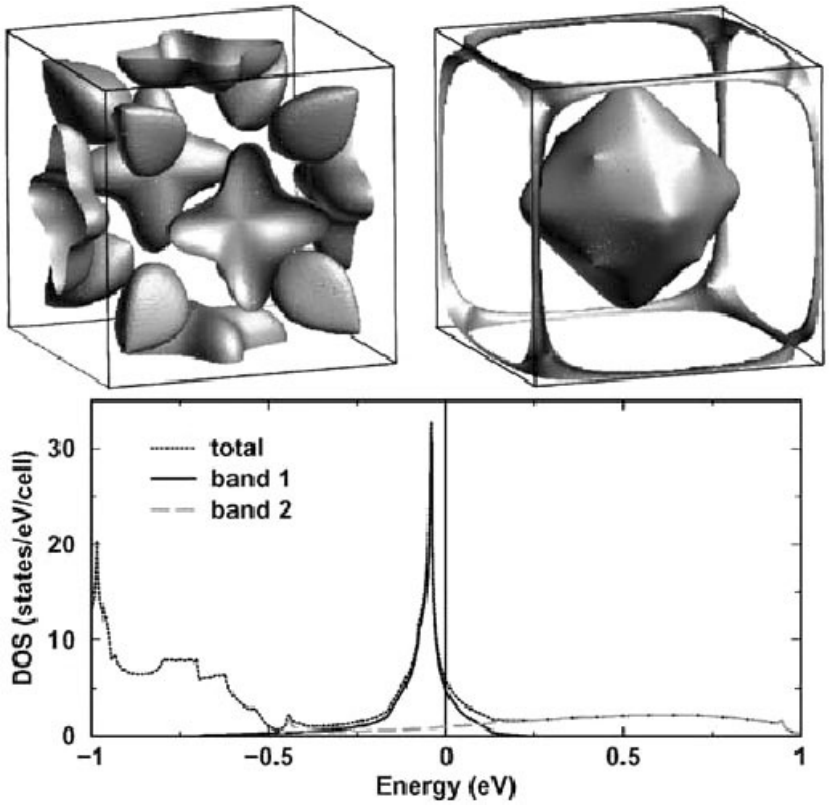

Figure 25. The two Fermi surface sheets of $MgCNi_3$ and the corresponding band resolved density of states near E_F. Band 1 corresponds to the Fermi surface sheet in the top right panel and band 2 corresponds to that of the top left panel [24].

in T_c [18]. The DOS of the two bands along with those of their Fermi surface sheets are shown in figure 25. A multi-band superconductor [111, 112] with a conventional phonon mechanism can develop an unconventional state with a non-trivial order parameter phase relation between the individual bands. It is proposed [69] that such a state can explain the experimentally found [9] s-wave pairing symmetry and unconventional superconductivity in $MgCNi_3$. It has been shown [69] that such a state gives rise to Andreev bound states and to spontaneous currents, at surfaces and around impurities, which can explain the zero-bias features observed in quasi-particle tunnelling [9].

10. Conclusions

The following conclusions can be drawn as regards the physics of $MgCNi_3$.

(1) It has a simple cubic perovskite structure [1] like the 30 K oxide non-cuprate superconductor $Ba_{1-x}K_xBiO_3$ with space group $Pm\bar{3}m$ and the lattice parameter a is $\sim$3.812 Å.

(2) The Ni K-edge x-ray absorption study [16] suggests that the $Ni_6(O_6)$ octahedra are locally distorted from those expected in the perfect cubic $Pm\bar{3}m$ form.

(3) It is found [5] that the compound has the perovskite structure over the temperature range (2–295 K) and no structural or long range magnetic ordering transitions are observed. Its structure is also stable under a pressure of ∼22 GPa [30].
(4) A high proportion of Ni in this compound indicates that the magnetic interactions may play a dominant role as regards its superconductivity.
(5) The superconducting transition temperature T_c of MgC_xNi_3 is sensitive to the carbon content increasing with x and $x \sim 1.45$–1.5 corresponds to the highest T_c [10, 12, 17, 56]. However, doping at the Mg and Ni sites decreases the T_c [6, 18, 33, 56] sharply.
(6) The external pressure increases the T_c of MgC_xNi_3 [17, 18] at the same rate as for other intermetallic superconductors but at a rate one order lower than that for MgB_2 and the pressure effect on T_c is independent of the C content.
(7) The ^{13}C NMR investigation on this material [3] implies that the electronic states reach a modestly mass enhanced Fermi-liquid-like state prior to the superconducting transition.
(8) Normal state NMR properties of $MgCNi_3$ are irregular [3] and analogous to those observed for the exotic superconductor Sr_2RuO_4.
(9) The change from grain boundary to core pinning by intragranular nanoparticles near T_c suggests [11] that the arrangement of pinning sites in $MgCNi_3$ is unique.
(10) Hall coefficient and thermoelectric power data [4, 7] on $MgCNi_3$ show that the carriers in this compound are electrons, in contrast to those of MgB_2. However, He *et al* [1] suggest that the holes in Ni d states might be responsible for the electrical conduction in this material in an electronic analogy to the holes in the O p states in perovskite oxide superconductors. The constant scattering approximation also shows that the thermoelectric power is hole type [50] above 10 K.
(11) It has been suggested [54] that $MgCNi_3$ is near a ferromagnetic instability and can be reached by hole doping at the Mg site (if 12% Mg is replaced by Na or Li, i.e., 0.04 hole/Ni).
(12) Energy band calculations [49–60] illustrate that the density of states (DOS) of the Fermi level (E_F) is dominated by Ni 3d states and there is a von Hove singularity (vHs) of the DOS [15, 54] just below the E_F (<50–120 meV). Nevertheless, photoemission and x-ray absorption studies [15] show that the sharp vHs peak theoretically predicted near E_F is substantially suppressed, which may be due to electron–electron and electron–phonon interactions.
(13) Both positive and negative magnetoresistances are reported [7, 16, 33], which needs further clarification.
(14) It has been observed [7] that the electronic contribution is slightly higher than the lattice one in the normal state thermal conductivity.
(15) $MgCNi_3$ is a single-gap superconductor in contrast to MgB_2 [100, 110] and the value of the superconducting gap (Δ) is estimated to be 1.1–1.5 meV [9, 13, 19, 47, 48], from tunnelling spectroscopy and specific heat data.
(16) The nuclear spin–lattice relaxation rate ($1/T_1$) displays the typical behaviour of isotropic s-wave superconductivity [3] for $MgCNi_3$ with a coherence peak below T_c. However, the field dependent specific heat and resistivity results imply that it is a moderate coupling, type-II, s-wave BCS superconductor [1, 11, 13, 14, 38, 47, 48]; this is supported by tunnelling and other experiments as well as theoretical calculations [19, 21, 49, 51, 67]. Again, the penetration depth distinctly exhibits a non-s-wave BCS low temperature behaviour [42], instead of showing a quadratic temperature dependence, suggestive of a nodal order parameter. It is also theoretically suggested that it is a d-wave superconductor [59]. Thus the nature of the superconductivity in $MgCNi_3$ is still controversial and needs more efforts to clarify it.

11. Future scope of work

(1) The single-crystal or wires/tapes form of $MgCNi_3$ should be studied to allow focusing on the changes of properties (if any) compared to those of the polycrystalline bulk and thin films.
(2) The nature of the superconductivity in $MgCNi_3$ should be clarified.
(3) The computation of some important parameters such as $\mathrm{d}\ln N(E_F)/\mathrm{d}P$ and $\mathrm{d}\ln\omega/\mathrm{d}P$ for MgC_xNi_3 may be useful for quantitative analysis of pressure dependent T_c data.
(4) The calculated optical properties should be experimentally verified.
(5) Intensive theoretical studies are needed to clarify the controversies over the type of the superconductivity and normal state magnetoresistance of $MgCNi_3$.

Acknowledgments

The author is grateful to his colleagues for their constant encouragement, support and constructive suggestions.

References

[1] He T *et al* 2001 *Nature* **411** 54
[2] Nagamatsu J, Nakagawa N, Muranaka T, Zenaitani Y and Akimitsu J 2001 *Nature* **410** 63
[3] Singer P M, Imai T, He T, Hayward M A and Cava R J 2001 *Phys. Rev. Lett.* **87** 257601
[4] Li S Y *et al* 2001 *Phys. Rev.* B **64** 132505
[5] Huang Q, He T, Regan K A, Rogado N, Hayward M, Hass M K, Inumaru K and Cava R J 2001 *Physica* C **363** 215
[6] Hayward M A, Hass M K, Ramirez A P, He T, Regan K A, Rogado N, Inumaru K and Cava R J 2001 *Solid State Commun.* **119** 491
[7] Li S Y *et al* 2002 *Phys. Rev.* B **65** 064534
[8] Li J Q, Wu L J, Li L and Zhu Y 2002 *Phys. Rev.* B **65** 052506
[9] Mao Z Q, Rosario M M, Nelson K D, Wu K, Deac I G, Schiffer P, Liu Y, He T, Regan K A and Cava R J 2003 *Phys. Rev.* B **67** 094502
[10] Ren Z A, Che G C, Jia S L, Chen H, Ni Y M and Zhao Z X 2001 *Preprint* cond-mat/0105366
Ren Z A, Che G C, Jia S L, Chen H, Ni Y M and Zhao Z X 2001 *Sci. China* A **44** 1205
[11] Cooley L D, Song X, Jiang J, Larbalestier D C, He T, Regan K A and Cava R J 2002 *Phys. Rev.* B **65** 214518
[12] Amos T G, Huang Q, Lynn J W, He T and Cava R J 2002 *Solid State Commun.* **121** 73
[13] Lin J-Y, Ho P L, Huang H L, Lin P H, Zhang Y-L, Yu R-C, Jin C-Q and Yang H D 2003 *Phys. Rev.* B **67** 052501
[14] Lin J-Y, Lin P H, Ho P L, Huang H L, Zhang Y-L, Yu R-C, Jin C-Q and Yang H D 2002 *J. Supercond.* **15** 485
[15] Kim J H, Ahn J S, Kim J, Park M-S, Lee S I, Choi E J and Oh S-J 2002 *Phys. Rev.* B **66** 172507
[16] Ignatov A Y, Dieng L M, Tyson T A, He T and Cava R J 2003 *Phys. Rev.* B **67** 064509
[17] Yang H D, Mollah S, Huang W L, Ho P L, Huang H L, Liu C-J, Lin J-Y, Zhang Y-L, Yu R-C and Jin C-Q 2003 *Phys. Rev.* B **68** 092507
[18] Kumary T G, Janaki J, Mani A, Jaya S M, Sastry V S, Hariharan Y, Radhakrishnan T S and Valsakumar M C 2002 *Phys. Rev.* B **66** 064510
[19] Kinoda G, Nishiyama M, Zhao Y, Murakami M, Koshizuka N and Hasegawa T 2001 *Japan. J. Appl. Phys.* **40** L1365
[20] Young D P, Moldovan M, Craig D D, Adams P W and Chan J Y 2003 *Phys. Rev.* B **68** 020501
[21] Liu F M, Li J Q, Dong C, Wang T M, Zhou Y Q and Chen H 2002 *Supercond. Sci. Technol.* **15** 1316
[22] Lin J-Y, Yang H D and Jin C-Q 2003 *Physica* C **388/389** 559
[23] Jin C Q, Zhang Y L, Liu Z X, Li F Y, Yu W and Yu R C 2003 *Physica* C **388/389** 561
[24] Rosner H *et al* 2003 *Physica* C **388/389** 563
[25] Wang H, Ouyang L Z, Zeng M Q and Zhu M 2004 *Scr. Mater.* **50** 1471
[26] Ferretti M, Ciccarelli C, Magnone E, Rubino S, Parodi N and Martinelli A 2004 *Mater. Res. Bull.* **39** 647
[27] Schaak R E, Avdeev M, Lee W L, Lawes L G, Zandbergen H W, Jorgensen J D, Ong N P, Ramirez A P and Cava R J 2004 *J. Solid State Chem.* **177** 1244

[28] Ren Z A, Che G C, Jia S L, Chen H, Ni Y M, Liu G D and Zhao Z X 2002 *Physica* C **371** 1
[29] Wei Z F, Chen X L, Che G C, Wang F M, Li W C and He M 2002 *Chin. Phys. Lett.* **19** 249
[30] Zhang Y L, Li F Y, Chen L C, Liu J, Yu R C, Liu Z X, Yu W and Jin C Q 2003 *Chin. Sci. Bull.* **48** 2287
[31] Artini C, Costa G A, Magnone E, Cimberle M R and Masini R 2003 *Int. J. Mod. Phys.* B **17** 819
[32] Kar'kin A E, Goshchitskii B N, Kurmaev E Z, Ren J A and Che G C 2003 *Phys. Met. Metallogr.* **95** 324
[33] Das A and Kremer R K 2003 *Phys. Rev.* B **68** 064503
[34] Alzamora M, Sanchez D R, Cindra M and Baggio-Saitovitch E M 2002 *Braz. J. Phys.* **32** 755
[35] Cooley L, Song X Y and Larbalestier D 2003 *IEEE Trans. Appl. Supercond.* **13** 3280
[36] Chen L, Li H and Mei L M 2004 *J. Mater. Sci. Technol.* **20** 203
[37] Chen L and Li H 2004 *Acta Phys. Sin.* **53** 922
[38] Park M S, Giim J S, Park S H, Lee Y W, Lee S I and Choi E J 2004 *Supercond. Sci. Technol.* **17** 274
[39] Wang C H, Mo W Q, Li S Y, Yu M, Fan R, Ruan K Q, Yang H S, Cao L Z and Chen X H 2002 *Acta Phys. Sin.* **51** 1816
[40] Yao Y X, Ying X N, Huang Y N, Wang Y N, Ren Z A, Che G C, Wen H H, Zhao Z X and Ding J W 2004 *Supercond. Sci. Technol.* **17** 608
[41] Park S H, Lee Y W, Giim J, Jung S H, Ri H C and Choi E J 2004 *Physica* C **400** 160
[42] Prozorov R, Snezhko A, He T and Cava R J 2003 *Phys. Rev.* B **68** 180502
[43] Shan L, Tao H J, Gao H, Li Z Z, Ren Z A, Che G C and Wen H H 2003 *Phys. Rev.* B **68** 144510
[44] Ouyang L Z, Wang H, Peng C H, Zeng M Q, Chung C Y and Zhu M 2004 *Mater. Lett.* **58** 2203
[45] Naidyuk Y G 2004 *Phys. Rev.* B **69** 136501
[46] Mao Z Q, Rosario M M, Nelson K D, Wu K, Deac I G, Schiffer P, Liu Y, He T, Regan K A and Cava R J 2004 *Phys. Rev.* B **69** 136502
[47] Shan L, Xia K, Liu Z Y, Wen H H, Ren Z A, Che G C and Zhao Z X 2003 *Phys. Rev.* B **68** 024523
[48] Waelte A, Fuchs G, Mueller K-H, Handstein A, Nenkov K, Narozhnyi V N, Drechsler S-L, Shulga S, Schultz L and Rosner H 2004 *Preprint* cond-mat/0402421
[49] Shim J H, Kwon S K and Min B I 2001 *Phys. Rev.* B **64** 180510
[50] Singh D J and Mazin I I 2001 *Phys. Rev.* B **64** 140507
[51] Dugdale S B and Jarlborg T 2001 *Phys. Rev.* B **64** 100508
[52] Szajek A 2001 *J. Phys.: Condens. Matter* **13** L595
[53] Shein I R, Ivanovskii A L and Medvedeva N I 2001 *JETP Lett.* **74** 122
[54] Rosner H, Weht R, Johannes M D, Pickett W E and Tosatti E 2002 *Phys. Rev. Lett.* **88** 027001
[55] Kim I G, Lee J I and Freeman A J 2002 *Phys. Rev.* B **66** 174512
[56] Shein I R, Ivanovskii A L, Kurmaev E Z, Moewes A, Chiuzbian S, Finkelstein L D, Neumann M, Ren Z A and Che G C 2002 *Phys. Rev.* B **66** 024520
[57] Kim I G, Lee J I and Freeman A J 2002 *Phys. Rev.* B **65** 064525
[58] Wang J L, Xu Y, Zeng Z, Zheng Q Q and Lin H Q 2002 *J. Appl. Phys.* **91** 8504
[59] Granada C M, Silva C M D and Gomes A A 2002 *Solid State Commun.* **122** 269
[60] Shein I R and Ivanovskii A L 2002 *J. Struct. Chem.* **43** 168
[61] Wu B M, Li B, Yang D S, Zheng W H, Li S Y, Gao L Z and Chen X H 2003 *Acta Phys. Sin.* **52** 3150
[62] Liu S, Shen R, Zheng Z M and Xing D Y 2003 *Chin. Phys. Lett.* **20** 284
[63] Heid R, Renker B, Schober H, Adelmann P, Ernst D and Bohnen K P 2004 *Phys. Rev.* B **69** 092511
[64] Wan X G, Weng H M and Dong J M 2002 *Chin. Phys. Lett.* **19** 1522
[65] Tan M Q, Tao X M, Xu X J, He J H and Ye G X 2003 *Acta Phys. Sin.* **52** 463
[66] Ignatov A Y, Savrasov S Y and Tyson T A 2003 *Phys. Rev.* B **68** 220504
[67] Tan M Q, Tao X M, Xu X J, He J H and Ye G X 2003 *Physica* B **337** 95
[68] Okoye C M I 2003 *J. Phys.: Condens. Matter* **15** 833
[69] Voelker K and Sigrist M 2003 *Preprint* cond-mat/0208367
[70] Yonemitsu K, Bishop A R and Lorenzana J 1993 *Phys. Rev.* B **47** 8065
[71] Schilling J S, Jorgensen J D, Hinks D G, Deemyad S, Hamlin J, Looney C W and Tomita T 2001 *Studies of High Temperature Superconductors* vol 38, ed A V Narlikar (New York: Nova Science) p 321
[72] Monteverde M, Nunez-Regueiro M, Rogado N, Regan K A, Hayward M A, He T, Loureiro S M and Cava R J 2001 *Science* **292** 75
[73] Lorenz B, Meng R L and Chu C W 2001 *Phys. Rev.* B **64** 012507
[74] Sato E, Taknenobu T, Ito T, Iwasa Y, Prassides K and Arima T 2001 *J. Phys.: Condens. Matter* **13** L267
[75] Schmidt H and Braun H F 1994 *Physica* C **229** 315
[76] Alleno E, Neumeier J J, Thompson J D, Canfield P C and Cho B K 1995 *Physica* C **242** 169
[77] Meenakshi S, Vijaykumar V, Rao R S, Godwal B K, Sikka S K, Ravindran P, Hossain Z, Nagarjan R, Gupta L C and Vijayaraghavan R 1998 *Phys. Rev.* B **58** 3377

[78] Weng S S, Hong I P, Chang C F, Tsay H L, Chatterjee S, Yang H D and Lin J-Y 1999 *Phys. Rev.* B **59** 11205
[79] Mani A, Bharathi A, Sastry V S, Hariharan Y and Radhakrishnan T S 2001 *ICEC18: Proc. 18th Int. Conf. on Cryogenic Engineering* ed K G Narayankhedkar (New Delhi: Narosa Publishing House) p 615
[80] McMillan W L 1968 *Phys. Rev.* **167** 331
[81] Ishizuka M, Iketani M and Endo S 2000 *Phys. Rev.* B **61** 3823
[82] Jennings L D and Swenson C A 1958 *Phys. Rev.* **112** 31
[83] Lin J-Y and Yang H D 2004 *Superconductivity Research at the Leading Edge* ed P S Lewis (New York: Nova Science) pp 111–30
[84] Werthamer N R, Helfand E and Hohenberg P C 1966 *Phys. Rev.* **147** 295
[85] Shulga S V and Drechsler S-L 2002 *J. Low Temp. Phys.* **129** 93
[86] Clogston A M 1962 *Phys. Rev. Lett.* **9** 266
[87] Chandrasekhar B S 1962 *Appl. Phys. Lett.* **1** 7
[88] Orlando T P, McNiff E J J, Foner S and Beasley M R 1979 *Phys. Rev.* B **19** 4545
[89] Kittel C 1996 *Introduction to Solid State Physics* 7th edn (New York: Wiley)
[90] Meingast C and Larbalestier D C 1989 *J. Appl. Phys.* **66** 5971
[91] Pippard A B 1989 *Magnetoresistance in Metals* (Cambridge: Cambridge University Press)
[92] Heeger A 1969 *Solid State Physics* vol 23 (New York: Academic) p 283
[93] Affronte M, Marcus J and Escribe-Filippini C 1993 *Solid State Commun.* **85** 501
[94] Anderson P W 1991 *Phys. Rev. Lett.* **67** 2092
[95] Sera M, Kobayash S, Hiroi M, Kobayashi N, Takeya H and Kadouaki K 1996 *Phys. Rev.* B **54** 3062
[96] Bauer E, Paul C, Berger S, Majumdar S, Michor H, Giovannini M, Saccone A and Bianconi A 2001 *J. Phys.: Condens. Matter* **13** L487
[97] Berman R 1976 *Thermal Conduction in Solids* (London: Oxford University Press)
[98] Kaiser A B 1987 *Phys. Rev.* B **35** 4677
[99] Nishizaki S, Maeno Y and Mao Z 2000 *J. Phys. Soc. Japan* **69** 572
[100] Yang H D, Lin J-Y, Li H H, Hsu F H, Liu C-J, Li S-C, Yu R-C and Jin C-Q 2001 *Phys. Rev. Lett.* **87** 167003
[101] Kresin V Z and Parkhomenko V P 1975 *Sov. Phys.—Solid State* **16** 2180
[102] Caroli C, Gennes P G D and Matricon J 1964 *Phys. Lett.* **9** 307
[103] Volovik G E 1993 *JETP Lett.* **58** 469
[104] For a brief review, see Yang H D and Lin J Y 2001 *J. Phys. Chem. Solids* **62** 1861
[105] Ramirez A P 1996 *Phys. Lett.* A **211** 59
[106] Sonier J E, Hundley M F and Brill J W 1999 *Phys. Rev. Lett.* **82** 4914
[107] Chen S J, Chang C F, Tsay H L, Yang H D and Lin J-Y 1998 *Phys. Rev.* B **58** 14753
[108] Chang C F, Lin J-Y and Yang H D 2000 *Phys. Rev.* B **61** 14350
[109] Cole K S and Cole R H 1941 *J. Chem. Phys.* **9** 311
[110] Mollah S, Yang H D and Chaudhuri B K 2003 *Ind. J. Phys.* A **77** 9
[111] Suhl H, Matthias B T and Walker L R 1959 *Phys. Rev. Lett.* **3** 552
[112] Agterberg D F, Barzykin V and Gor'kov L P 1999 *Phys. Rev.* B **60** 14868